Simplified Electromagnetic Method for the Analytical Euclidean Modeling of Multiple Electrical Conductors in Arbitrary Directions

Dorindo Cardenas*, Sherlie Portugal and Alejandro Von Chong

School of Electrical Engineering, Universidad Tecnológica de Panamá, Campus Víctor Levi Sasso, Panama City, P.O. Box 0819-07289, Panama

INFORMATION

Keywords:
Electric field
magnetic field
multiple infinite conductors
linear currents
analytic method
vector space solutions
Euclidean space

DOI: 10.23967/j.rimni.2025.10.65324

SCIPEDIA Revista Internacional de Métodos Numéricos para Cálculo y Diseño en Ingeniería

Revista Internacional Métodos numéricos para cálculo y diseño en ingeniería RIMNI

In cooperation with CIMNE

Simplified Electromagnetic Method for the Analytical Euclidean Modeling of Multiple Electrical Conductors in Arbitrary Directions

Dorindo Cardenas*, Sherlie Portugal and Alejandro Von Chong

School of Electrical Engineering, Universidad Tecnológica de Panamá, Campus Víctor Levi Sasso, Panama City, P.O. Box 0819-07289, Panama

ABSTRACT

The analytical modeling of electromagnetic fields generated by multiple current-carrying conductors is fundamental in power systems, electromagnetic compatibility, and transmission line analysis. Traditional analytical methods often assume conductors aligned with the coordinate system axes, limiting their applicability to arbitrary configurations. This paper presents a novel analytical approach that determines the exact electric and magnetic fields for multiple conductors oriented in arbitrary directions within a Euclidean space, assuming linear, homogeneous, and isotropic media. Unlike numerical methods, such as the Finite Element Method (FEM), which require extensive meshing and domain discretization, the proposed method directly computes field vectors without interpolation or artificial boundary conditions. The applicability of the method is evaluated through four case studies, demonstrating its effectiveness in various configurations, including power transmission lines, communication cables, and grounding systems in homogeneous isotropic media. Additionally, a comparative analysis is performed using a specific case with a known analytical solution, validating the method against FEM-based solvers such as ANSYS Maxwell and FEMM. The results confirm that the proposed approach achieves higher accuracy with significantly lower computational costs.

OPEN ACCESS

Received: 10/03/2025

Accepted: 09/06/2025

Published: 30/06/2025

DOI
10.23967/j.rimni.2025.10.65324

Keywords:
Electric field
magnetic field
multiple infinite conductors
linear currents
analytic method
vector space solutions
Euclidean space

1 Introduction

It has been more than 150 years since James Clerk Maxwell presented the paper "A Dynamical Theory of the Electromagnetic Field" [1], summarizing and unifying all previous physical and mathematical findings related to electric and magnetic phenomena, and formally unifying the laws of Gauss, Ampère and Faraday. These principles became the foundation for calculating electromagnetic fields emanating from all sorts of electrical systems, many of which conform with geometries such as spheres, loops, and very long lines, hence the general interest in the electromagnetic characterization of these shapes.

*Correspondence: Dorindo Cardenas (dorindo.cardenas@utp.ac.pa). This is an article distributed under the terms of the Creative Commons BY-NC-SA license

For configurations modeled as infinite current-carrying lines, the classical analytical solution for electric and magnetic fields relies on Gauss's and Ampere's Laws. However, this approach assumes that the conductor's direction, which defines both the axis of the cylindrical Gaussian surface and the rotation of the Ampere loop, coincides with one of the reference coordinate system's axes. However, it is not possible to keep this assumption for multiple lines, unless a different reference system is used for each of them, which becomes complex and tedious, but in practice it is what we have in electrical distribution systems from many countries. Such a case would require the individual solution of each line in its own reference system to then superimpose individual effects at each spatial point of interest using a geometric approximation method between individual systems, but since the number of calculations required increases rapidly, due to the superposition and transformation operations required for each conductor's individual coordinate system [2,3], this type of solution becomes cumbersome.

Accurately modeling the electromagnetic fields generated by multiple arbitrarily oriented conductors is crucial in power transmission, communication systems, and grounding networks. Traditional analytical methods are limited by symmetry assumptions, while Finite Element Method (FEM)-based numerical approaches require extensive meshing and high computational resources, particularly when modeling long conductors [4,5]. The proposed method provides a direct analytical formulation that eliminates the need for numerical discretization, offering an efficient and exact solution under the assumption of linear, homogeneous, and isotropic media, which is a common condition in engineering applications. By computing electric and magnetic field vectors directly at each point, it reduces interpolation errors and computational complexity, making it particularly useful for analyzing power distribution lines, long transmission cables, and electromagnetic interference in complex conductor arrangements. This approach is especially advantageous in scenarios where Finite Element Method (FEM) suffers from boundary truncation errors and increased computational costs due to the need for large simulation domains.

In classical Electromagnetics, the electromagnetic field of an infinite line of current is solved by applying Gauss's and Ampere's Law, while conveniently placing the current-carrying wire over the z-axis in the cylindrical coordinate system to take advantage of the resultant symmetry [6,7]. However, this simple strategy no longer applies when dealing with more than one conductor, especially if the directions of the currents are not parallel, because we only have a single z-axis. Some authors have applied analytical models to specific areas of research, but their solutions are still limited to the case of a single line [8,9], and even if some advanced publications offer certain analytical solutions for the electromagnetic field along infinite lines with the intervention of external fields or other charges, they are based on specific conditions and assumptions to ensure a symmetric analysis; therefore, they cannot be considered general analytical methods [10,11]. A combined method that could be used starts by solving the fields foreach of the conductors in its own Euclidean system and then uses the resultants of each of the individual contributions of the fields as matrices (vectors) translated and rotated towards the main system of reference. This seems to be the best analytical method that currently provides a general solution for these cases. This methodology is impractical and demanding in terms of the amount of mathematical work, since with each cable a complete reference system must be handled in addition to the main reference system, for which the calculations are desired. Therefore, the greater the number of cables, the greater the number of reference systems required and the mathematical complexity, since results at each point must be rotated and translated to that main reference system in which the total effect can be represented. Finally, one could use the equations governing electrical and magnetic interactions in their differential form to calculate the total fields at

a point of interest through integration, but in this case, close-form solutions are only possible for well-known symmetric geometries [12]; therefore, this path is usually reserved for computational models, which offer numerical approximations [13,14].

Most medium and high voltage transmission lines (1 kV and above) are made of bare conductors (air insulation only), whereas low voltage transmission lines (1000 volts or less) and conductors engineered for undergrounding are insulated according to the standard NFPA 70-Chapter 3 [15] for most countries in the American continent and IEC 60364 [16] for most of Europe and various territories in Asia, Africa, and Oceania, because they are easily accessible by unqualified personnel. Although the insulation is composed of different layers, these are symmetrical around the conductor and their materials can be considered linear, homogeneous, and isotropic [17–21].

In practice, precise information about the current and other electrical signals in each conductor is easily obtainable by measurement devices strategically located in the electrical network (current transformers or CTs), as well as meters of the different energy classifications used in engineering (real, reactive, apparent). This data, gathered through a Supervisory Control and Data Acquisition system (SCADA), can be interpreted through Graphs and mathematical functions, providing a complete real-time description of the current in each conductor of the entire electrical system [22,23].

Since the data is measured from the real-time operation of the transmission line, all interactions between electrical charges or currents inside the conductors are intrinsically included (coupling phenomena, mutual inductances or capacitances, proximity effects, reflections, resistivity variations, etc.) and the functions or phasors of current can be written directly from it. For the purposes of calculating the external fields to the conductors in a practical way, a linear system can be considered as the sum of the effects produced by each one of the currents already measured, which have fixed positions in the system.

Until now, in the applied fields of electrical engineering, the electromagnetic field due to a plural number of lines of current can be generally estimated through Computational Electromagnetics (CEM) techniques, which offer approximated numerical values for points of interest [24,25]. However, a gap remains in the literature regarding analytical electromagnetic models able to yield summarized "Gauss-Ampere type" expressions for systems or cases that need to be analyzed in a comprehensive manner. Therefore, in this work we introduce an efficient analytical method for computing the electromagnetic field generated by multiple infinite current-carrying conductors with arbitrary spatial directions, which can be used even without the help of computational elements and can provide exact solutions, not only the usual approximate solutions of computational calculation. This method is applicable and of special interest in several fields such as telecommunications, aviation, and healthcare, where electromagnetic interference (EMI) can compromise essential systems. In telecommunications, EMI from transmission lines can degrade signal integrity, leading to data loss and system malfunctions [26]. In aviation, EMI can disrupt avionics systems, interfering with cockpit radios and radar signals, essential for communication and navigation [27]. Research on electromagnetic interference and compatibility in aeronautical radio communication systems emphasizes the need for effective EMI mitigation measures to ensure flight safety [28]. Similarly, in medical facilities, EMI from transmission lines can degrade the performance of sensitive devices like MRI machines and pacemakers, potentially jeopardizing patient safety [29]. Predictive modeling through electromagnetic analysis aids in optimizing emitting devices, shielding sensitive instruments, and ensuring the safe integration of external sources near medical tools like MRI systems [30]. By providing a precise and computationally efficient solution, this method offers a novel approach to enhancing system reliability and safety in these sectors.

2 Methods

The deduction of the method being introduced starts with the basic analysis of an infinite current-carrying wire, as illustrated in Fig. 1. The infinity of the wire is a valid assumption for space points around long conductors.

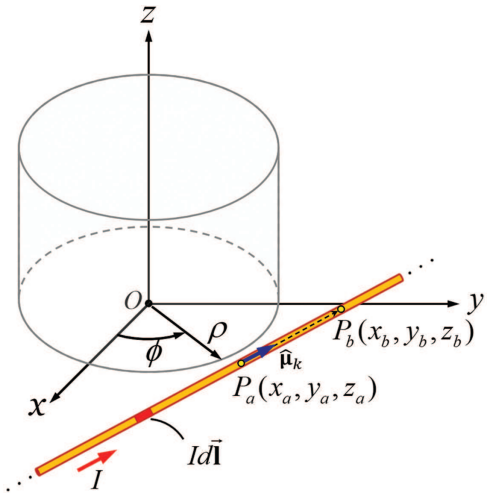

Figure 1: Single current-carrying wire following an arbitrary direction defined by the unit vecto $\hat{\mu}_k$

Inside the wire, the charges move with a drift velocity $\vec{v}_d = v_d\hat{\mu}_k$, and the electric charge density related to the electric current λ_m called conduction charge, can be considered linear and constant since the materials of the conductor cables are linear, homogeneous, isotropic and the diameter is constant. When all charge density can be considered conduction charge, and the ratio of the diameter d to the length ℓ of the wire is such that the diameter becomes very small with respect to its length, or with respect to the external points of interest for the calculation of the fields, so it can be considered of infinite length, the current I is given by (1).

$$I = \lambda_m v_d \tag{1}$$

Instead of following the classical approach, which places the wire along the z axis in cylindrical coordinates, we allow the wire to align with an arbitrary unit vector $\hat{\mu}_k$. This vector may differ from the standard unit vectors in cylindrical coordinates: $\hat{\mu}_\rho$, $\hat{\mu}_\phi$ and $\hat{\mu}_z$.

The $\hat{\mu}_k$ vector is obtained from two points positioned over the line of the wire, here identified as $P_a(x_a, y_a, z_a)$ and $P_b(x_b, y_b, z_b)$ as shown in Fig. 1. The vector containing the spatial displacement between said points $\overrightarrow{P_aP_b}$ is calculated and then divided by its magnitude, as shown in (2).

$$\hat{\mu}_k = \frac{\vec{P_aP_b}}{\left\|\vec{P_aP_b}\right\|}$$

$$\hat{\mu}_k = \frac{(x_b - x_a)\hat{\mu}_x + (y_b - y_a)\hat{\mu}_y + (z_b - z_a)\hat{\mu}_z}{\sqrt{(x_b - x_a)^2 + (y_b - y_a)^2 + (z_b - z_a)^2}} \tag{2}$$

The electric field vector $\vec{E}$ is oriented in the radial direction perpendicular to the wire, which has a unit vector defined as $\hat{\mu}_r$. An expression for the electric field is obtained with the application of Gauss's Law, as shown in (3), where $\vec{D}$ is the electric displacement field and λ is the value per unit length of

the charges responsible for the electric field, that is, those that are considered on the surface of the conductor. A cylindrical gaussian surface is stablished around the conducting wire, whose longitudinal axis corresponds to the direction of the wire $\hat{\boldsymbol{\mu}}_k$ while the unit vector of the axis of rotation is identified as $\hat{\boldsymbol{\mu}}_{\phi'}$. If one desires to know the magnitude of the electric field at a point of interest $P_i(x_i, y_i, z_i)$, the radius of the gaussian surface is adjusted to have the same value as the perpendicular distance between the wire and P_i, defined here as r_o. Therefore, the differential surface in (3) can be defined as $d\vec{s}_{r_o} = r_o d\phi' dl \hat{\boldsymbol{\mu}}_r$, a concept that is carefully illustrated in Fig. 2.

$$\oiint \vec{\mathbf{D}} \cdot d\vec{s}_{r_o} = \int \lambda dl \tag{3}$$

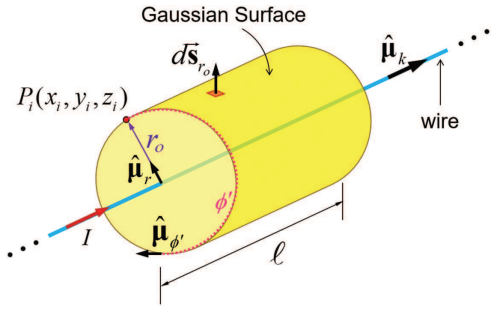

Figure 2: Gaussian surface enclosing a section of a linear conductor along the arbitrary direction $\hat{\boldsymbol{\mu}}_k$

After moving the invariable terms out of the integral and integrating the angular variable, the differential length on both sides of the equation can be canceled out, resulting in the simple expression presented in (4) to (4b).

$$\oiint \vec{\mathbf{D}} \cdot r_o d\phi' dl \hat{\boldsymbol{\mu}}_r = \int \lambda dl \tag{4}$$

$$D_{r_o} r_o 2\pi \int dl = \lambda \int dl \tag{4a}$$

$$D_r = \frac{\lambda}{2\pi r} \tag{4b}$$

Considering a linear, homogeneous, and isotropic medium; the electric field is expressed by (5).

$$\vec{\boldsymbol{E}} = \frac{\lambda}{2\pi \varepsilon r_o} \hat{\boldsymbol{\mu}}_r \tag{5}$$

where ε represents the electrical permittivity of the material.

Since not all electrical charge can always be considered free charge, or conduction charge, the most appropriate way to determine λ is through the actual parameters of the power line being considered. There are several engineering methods to model power lines from the data obtained from SCADA, so that the equivalent capacitance C_λ of the line and its voltage V_λ can be obtained [22,24]. Taking these values for each line, the electrical charge component Q_λ, which is considered superficial, can also be obtained as shown in (6). A linear distribution of this charge, which is linked to the electric field, is expressed as shown in (7).

$$Q_\lambda = C_\lambda V_\lambda \tag{6}$$

$$\lambda = \frac{Q_\lambda}{\ell} \tag{7}$$

Simultaneously, an expression for the magnetic field induced by the current in the wire is obtained through Ampere's Law in the analysis shown below with the resulting expressions (8) to (8b), and (9), where μ is the magnetic permeability corresponding to a linear, homogeneous, and isotropic medium.

$$\oint \vec{\boldsymbol{H}} \cdot d\vec{\boldsymbol{l}} = I \tag{8}$$

$$\oint \vec{\boldsymbol{H}} \cdot \left(r_o d\phi \hat{\boldsymbol{\mu}}_{\phi'}\right) = I \tag{8a}$$

$$H_{\phi'} = \frac{I}{2\pi r_o} \tag{8b}$$

$$\vec{\boldsymbol{B}} = \frac{\mu I}{2\pi r_o} \hat{\boldsymbol{\mu}}_{\phi'} \tag{9}$$

The next step is to establish a general form to obtain the perpendicular displacement vector from the wire to P_i; i.e., $\vec{\boldsymbol{r}}_o$. First, we measure the displacement from any given point in the wire P_λ to the point of interest P_i. The resulting vector $\vec{P_\lambda P_i}$ has a component in the direction orthogonal to the wire $\hat{\boldsymbol{\mu}}_r$, whose magnitude $||\vec{P_\lambda P_i}|| \sin\theta$ corresponds to r_o. Here θ is the angle between $\vec{P_\lambda P_i}$ and the wire. This is illustrated carefully illustrated in Fig. 3.

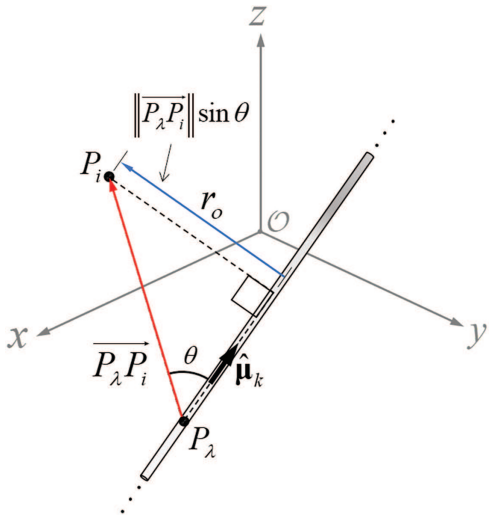

Figure 3: Trigonometric relationship to obtain the perpendicular distance from the wire to P_i

Since the cross product between any two vectors $\vec{\boldsymbol{A}}$ and $\vec{\boldsymbol{B}}$ is defined as $\hat{\boldsymbol{\mu}}_n AB \sin\theta$, where $\hat{\boldsymbol{\mu}}_n$ is the unit vector perpendicular to both $\vec{\boldsymbol{A}}$ and $\vec{\boldsymbol{B}}$, we can determine r_o through the cross product of $\hat{\boldsymbol{\mu}}_k$ and $\vec{P_\lambda P_i}$. We will use the orthogonal-orthonormal convention, summarized in the "right-hand rule" for cross products, in determining the final directions of the products. The result of this operation is a vector $\vec{\boldsymbol{r}}_{\phi'}$ (10) with magnitude equal to r_o, but whose direction follows $\hat{\boldsymbol{\mu}}_{\phi'}$.

$$\vec{\boldsymbol{r}}_{\phi'} = \hat{\boldsymbol{\mu}}_k \times \vec{P_\lambda P_i} = \hat{\boldsymbol{\mu}}_{\phi'} \left\|\vec{P_\lambda P_i}\right\| \sin\theta$$

$$\vec{\boldsymbol{r}}_{\phi'} = \hat{\boldsymbol{\mu}}_{\phi'} r_o \tag{10}$$

Then, $\vec{\boldsymbol{r}}_o$ is easily computed through the cross product of $\vec{\boldsymbol{r}}_{\phi'}$ and $\hat{\boldsymbol{\mu}}_k$, as indicated by (11).

$$\vec{\boldsymbol{r}}_o = \vec{\boldsymbol{r}}_{\phi'} \times \hat{\boldsymbol{\mu}}_k = \hat{\boldsymbol{\mu}}_{\phi'} r_o \times \hat{\boldsymbol{\mu}}_k$$

$$\vec{\boldsymbol{r}}_o = \hat{\boldsymbol{\mu}}_r r_o \tag{11}$$

The analysis carried out for a single line or straight wire can be extended to n number of lines, being n an integer between 1 and infinity, by making use of the superposition theorem. Thus, hereafter the subscript j will be used to indicate fields and parameters associated to the j^{th} line among all n lines being studied in a given problem. This means that j^{th} line is their "specific fields source". In a similar manner, the subscript i will signal a specific point in space where the fields are being measured. This notation is shown in Eqs. (12)–(16), where the link given by Eq. (14) is valid only when we can consider that all the electrical charge of the conductor is conduction charge. When this condition is not met, the determination of the linear charge density is carried out via Eq. (7).

$$\vec{\boldsymbol{E}}_{(i,j)} = \frac{\lambda_j}{2\pi\varepsilon r_{o(i,j)}} \hat{\boldsymbol{\mu}}_{r(i,j)} \tag{12}$$

$$\vec{\boldsymbol{B}}_{(i,j)} = \frac{\mu I_j}{2\pi r_{o(i,j)}} \hat{\boldsymbol{\mu}}_{\phi'(i,j)} \tag{13}$$

$$I_j = \lambda_{mj} v_{d_j} \tag{14}$$

$$\hat{\boldsymbol{\mu}}_{\phi'(i,j)} = \frac{\vec{\boldsymbol{r}}_{\phi'(i,j)}}{\left\| \vec{\boldsymbol{r}}_{\phi'(i,j)} \right\|} \tag{15}$$

$$\hat{\boldsymbol{\mu}}_{r(i,j)} = \frac{\vec{\boldsymbol{r}}_{o(i,j)}}{\left\| \vec{\boldsymbol{r}}_{o(i,j)} \right\|} \tag{16}$$

With the established notation, we can generalize the procedure to calculate the radial displacement from the j^{th} wire to any given point of interest P_i. This displacement vector $\vec{\boldsymbol{r}}_{o(i,j)}$, is always perpendicular to the direction of the wire $\hat{\boldsymbol{\mu}}_{k(j)}$ regardless of its orientation $\hat{\boldsymbol{\mu}}_{k(j)}$ is obtained from any two points over the j^{th} line or wire, following the same procedure as shown in (2). In addition, the displacement vector between a particular point along the j^{th} line $P_{\lambda_j}(x_{\lambda_j}, y_{\lambda_j}, z_{\lambda_j})$ and P_i is represented as $\vec{P_{\lambda_j} P_i}$. The cross product of $\hat{\boldsymbol{\mu}}_{k(j)}$ and $\vec{P_{\lambda_j} P_i}$ is used to calculate the vector $\vec{\boldsymbol{r}}_{\phi'(i,j)}$, whose magnitude equals $r_{o(i,j)}$, and then, $\vec{\boldsymbol{r}}_{o(i,j)}$ is determined through the cross product of $\vec{\boldsymbol{r}}_{\phi'(i,j)}$ and $\hat{\boldsymbol{\mu}}_{k(j)}$, in a similar way to what was done for (10) and (11); see (17) and (18).

$$\vec{\boldsymbol{r}}_{\phi'(i,j)} = \hat{\boldsymbol{\mu}}_{k(j)} \times \vec{P_{\lambda_j} P_i} = \hat{\boldsymbol{\mu}}_{\phi'(i,j)} r_{o(i,j)} \tag{17}$$

$$\vec{\boldsymbol{r}}_{o(i,j)} = \vec{\boldsymbol{r}}_{\phi'(i,j)} \times \hat{\boldsymbol{\mu}}_{k(j)} = \hat{\boldsymbol{\mu}}_{r(i,j)} r_{o(i,j)} \tag{18}$$

Finally, the analytical calculation for the electric and magnetic fields due to the n number of straight conductors is completed through superposition, as indicated in (19) and (20).

$$\vec{\boldsymbol{E}}_{(i)\text{total}} = \sum_{j=1}^{n} \vec{\boldsymbol{E}}_{(i,j)} = \sum_{j=1}^{n} \frac{\lambda_j}{2\pi\varepsilon r_{o(i,j)}} \hat{\boldsymbol{\mu}}_{r(i,j)} \tag{19}$$

$$\vec{\boldsymbol{B}}_{(i)\text{total}} = \sum_{j=1}^{n} \vec{\boldsymbol{B}}_{(i,j)} = \sum_{j=1}^{n} \frac{\mu I_j}{2\pi r_{o(i,j)}} \hat{\boldsymbol{\mu}}_{\phi'(i,j)} \tag{20}$$

3 Results

In the previous procedure, a reduced method is shown to analytically calculate the electric and magnetic fields at a particular point in space for any complex problem of multiple infinites charged lines and in arbitrary directions, using a single reference system.

This method is powerful, yet simple and convenient, since it only requires a small number of straightforward equations, avoiding the need for more sophisticated geometric or numerical computation algorithms. The analysis could be done manually in very simple cases or aided by a computer algorithm in complex scenarios. In the latter option, the computer algorithm is kept simple and short since it only needs to solve Eqs. (12)–(20), and it does not require further geometric manipulation of the results due to the absolute reference frame. An example of a developed algorithm for a complex case can be found in Appendix A. Several case studies implemented in MATLAB are presented to demonstrate the advantages of the proposed method.

3.1 Case Study 1

Here we consider a very long line of current in an arbitrary direction, passing through the points $P_a(12,-20,-60)$ and $P_b(10,40,60)$. The line carries an instantaneous current of 200 A and the surrounding medium is assumed to be linear, homogeneous and isotropic. Using the equivalent capacitance of a transmission line and its operating voltage (obtained through SCADA system monitoring) Eqs. (6) and (7) are applied to determine the linear electric charge distribution, which is directly related to the electric field along the line. In this case, a single conductor from a typical 115 kV three-phase transmission line used in American power systems is considered, with a length of 1 km and an equivalent capacitance of 5.767130 nF between lines. Based on SCADA-measured data, the estimated linear charge density on the conductor is $\lambda = 0.66667\times10^{-6}\frac{C}{m}$. A simple MATLAB [31] script has been generated to obtain the results of 1000 points using Eqs. (12)–(20). The calculation points have been arranged equidistantly in 10 layers of 100 points each in a Euclidean space of dimensions: $-50 \leq x \leq 50$, $-50 \leq y \leq 50$, $-50 \leq z \leq 50$. The resulting electrical $\vec{\boldsymbol{E}}$ field is depicted in Fig. 4, while the magnetic $\vec{\boldsymbol{B}}$ field is shown in Fig. 5. It can be noted that the forms of the electric and magnetic fields due to the line, are the expected ones according to the classical field theory, and the calculation and graphing have been achieved with ease, regardless of the arbitrary direction of the line.

3.2 Case Study 2

This case considers two very long lines of current ($n = 2$). Both currents follow the $\hat{\boldsymbol{\mu}}_z$ direction and are equidistant from the origin of the reference system; one passing through the point $(x,y,z) = (42.5,-42.5,0)$ and the other passing through $(x,y,z) = (-42.5,42.5,0)$. The intensity of both currents is 150 Amperes, and this case considers an estimated linear charge density on the power cables of $\lambda = 0.5\times10^{-6}\frac{C}{m}$. According to the symmetry of the problem, the fields must be zero along the z axis at the origin. These anticipated results serve to verify the effectiveness of the proposed analytical method. Comparable case studies have also been addressed with solution methods suggested by other authors; however, they have the disadvantage of only being valid under certain symmetrical conditions such as the one we see in this case [32–34], very specific applications, strong computational requirements or very approximate experimental data [35–37]. Although these cases are quite notorious, they could not yet be considered as solutions of a general case with electrical currents in any direction.

This time, the solution was evaluated over 4000 points using MATLAB [31]. Two different views of the resulting electric field are depicted in Figs. 6 and 7, which show that, as expected, the electric field disappears towards the center between both lines, *i.e.*, any point $(0,0,z)$.

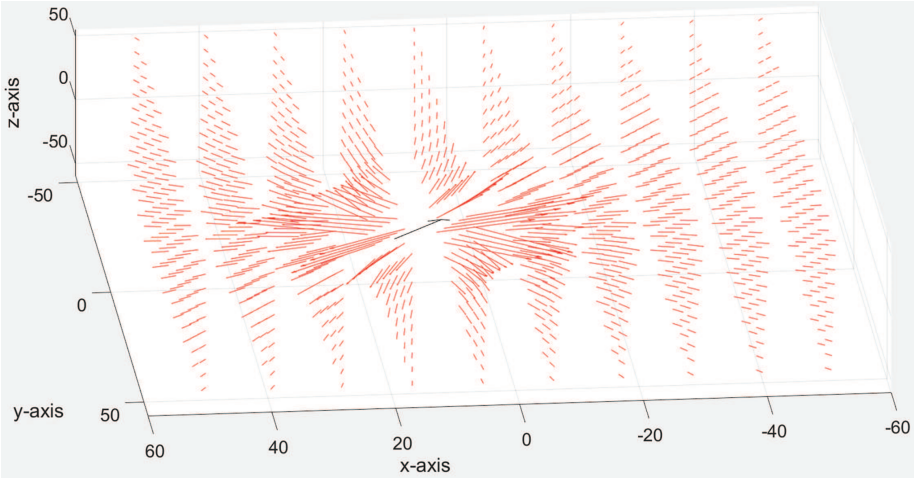

Figure 4: $\vec{\mathbf{E}}$ for Case Study 1 viewed from a perspective that shows the expected radial behavior of the field

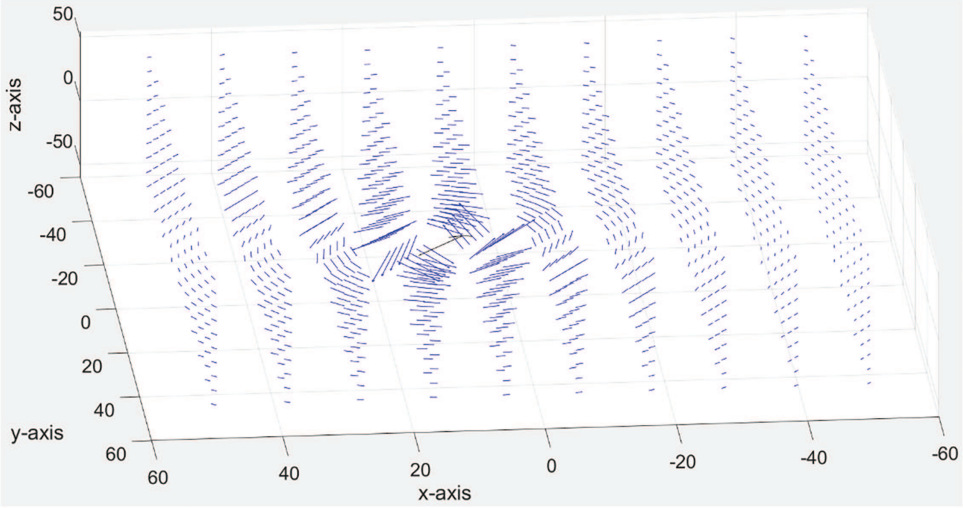

Figure 5: $\vec{\mathbf{B}}$ for Case Study 1 viewed from a perspective that shows the expected rotational behavior of the field

As for the magnetic field, two different views of the results, presented in Figs. 8 and 9, show that the field converges towards zero at half distance between both lines.

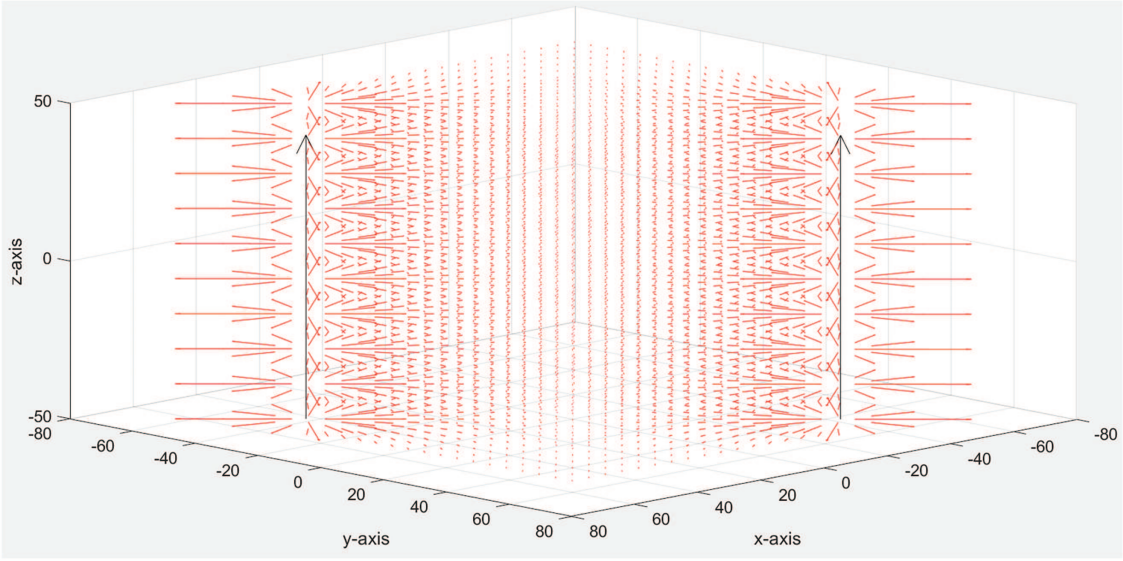

Figure 6: Three-dimensional graph of the resultant $\vec{\mathbf{E}}$ field for Case Study 2. The black lines represent the parallel electrical currents

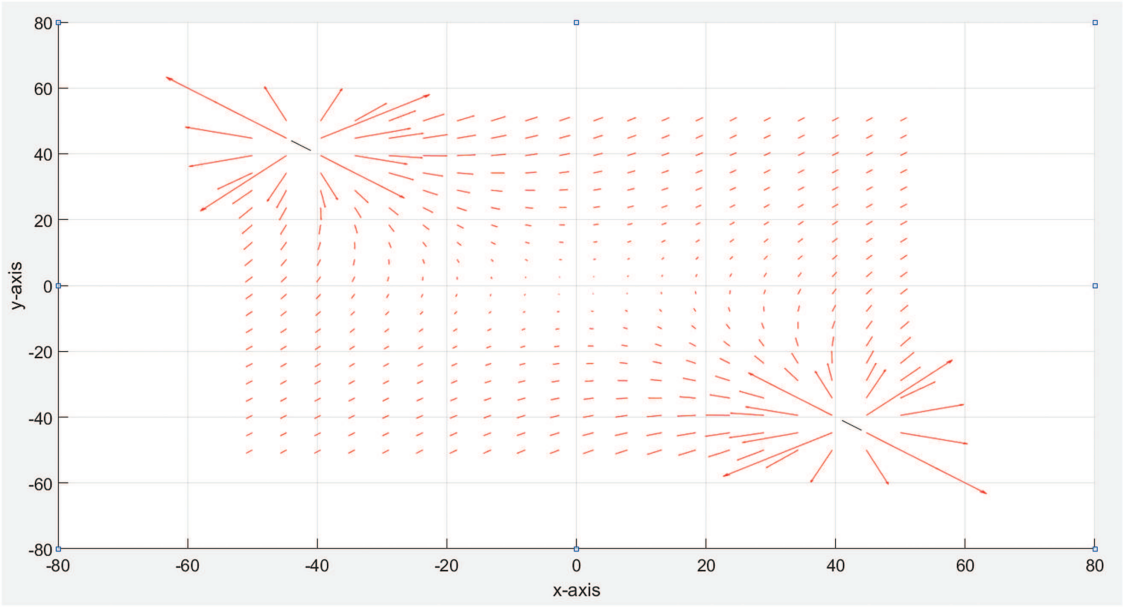

Figure 7: The $\vec{\mathbf{E}}$ field for Case Study 2 seen from the $+z$ axis (xy plane)

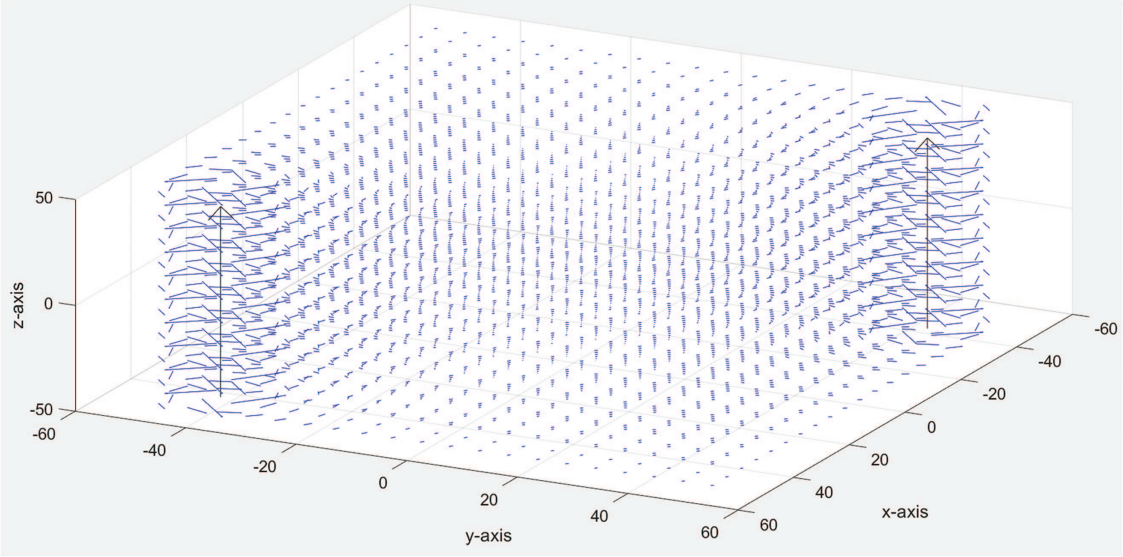

Figure 8: Three-dimensional graph of the resultant $\vec{\mathbf{B}}$ field for Case Study 2

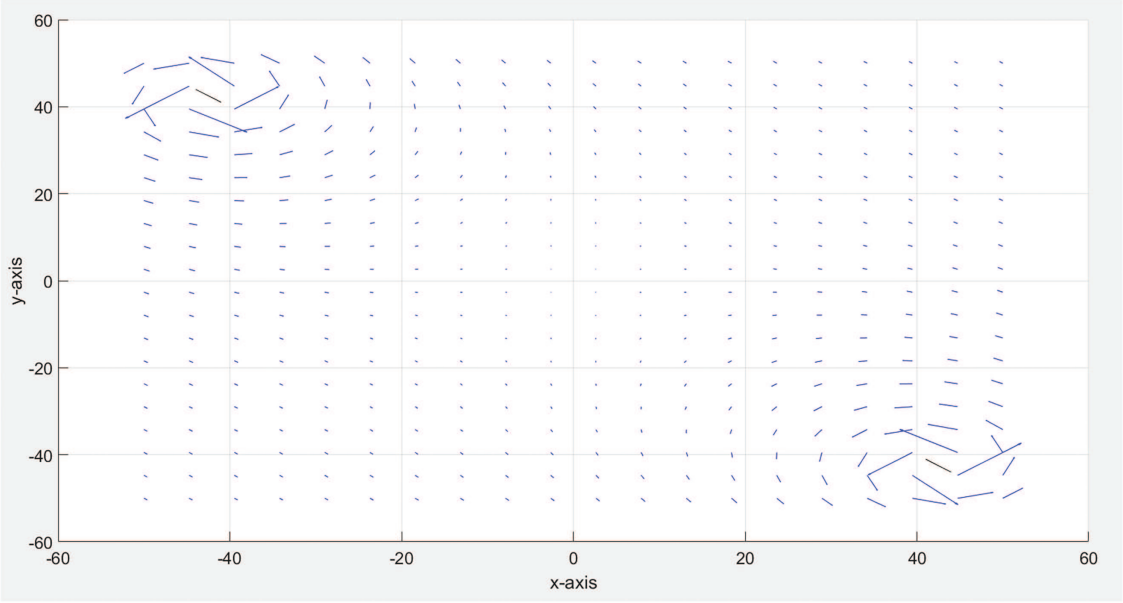

Figure 9: The $\vec{\mathbf{B}}$ field for Case Study 2 seen from the $+z$ axis (xy plane)

3.3 Case Study 3

This time, we consider three very long lines of current ($n = 3$) in different arbitrary directions. The first linear current $i(t)_{(1)}$ crosses the space points $P_a(-55,-25,55)$ and $P_b(55,-45,55)$, $i(t)_{(2)}$ passes through $P_c(15,0,-55)$ and $P_d(25,0,55)$, whereas $i(t)_{(3)}$ crosses $P_e(-45,55,-55)$ and $P_f(-35,-55,-55)$. The general intensities of the three currents are given by: $i(t)_{(1)} = 300\cos(\omega t)$, $i(t)_{(2)} = 350\sin\left(\omega t - \frac{\pi}{2} rad\right)$, and $i(t)_{(3)} = 400\cos(\omega t)$. However, in a steady state, the current

function can be translated from the time domain to the frequency domain (complex amplitude) [38]. Under the criterion of conservation of energy, we must express the current magnitudes in the frequency domain, as an effective and invariant magnitude, so it is necessary to also use the root mean square (RMS) concept for the magnitudes. Taking these considerations, we can write these currents as classical phasors: $I_{(1)} = \frac{300}{\sqrt{2}}\angle 0°$, $I_{(2)} = \frac{350}{\sqrt{2}}\angle 180°$, and $I_{(3)} = \frac{400}{\sqrt{2}}\angle 0°$. The solution of the electric and magnetic field was evaluated over a thousand equally spaced points in a Euclidean space of dimensions: $-50 \leq x \leq 50$, $-50 \leq y \leq 50$, $-50 \leq z \leq 50$ using MATLAB [31]. As each conductor has its own internal line parameters, three different charge densities have been considered in this case, $\lambda_{(1)} = 0.70711 \times 10^{-6}\frac{C}{m}$, $\lambda_{(2)} = 0.82496 \times 10^{-6}\frac{C}{m}$, and $\lambda_{(3)} = 0.94281 \times 10^{-6}\frac{C}{m}$ respectively for conductors carrying $I_{(1)}$, $I_{(2)}$ and $I_{(3)}$.

This case allows us to see in a practical way the great versatility and capacity of simplified modeling that the proposed method has. The results of this case are widely shown in Figs. 10–17. The proposed method is general and applicable to any number of current conducting lines, in any direction; and the results will be obtained jointly using a single reference system, either in an exact analytical way, or numerically by evaluating Eqs. (12)–(20), without additional requirements for any geometric manipulation, nor separate evaluations of fields that later require applying some type of rotation or translation of resultant vectors or matrices. In addition, symmetric models that could be used as an alternative in Case Study 2, would not work for a problem like Case Study 3.

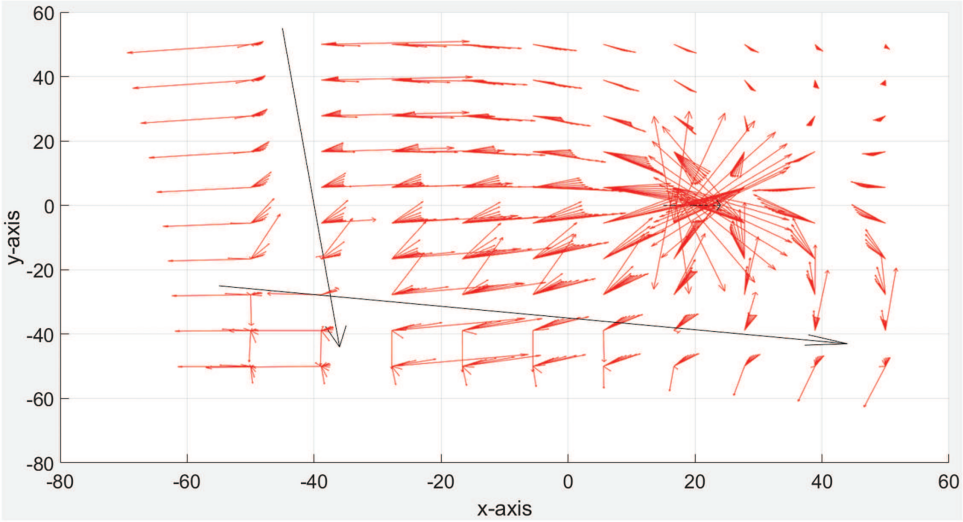

Figure 10: The $\vec{\mathbf{E}}$ field for Case Study 3 seen from the $+z$ axis (xy plane)

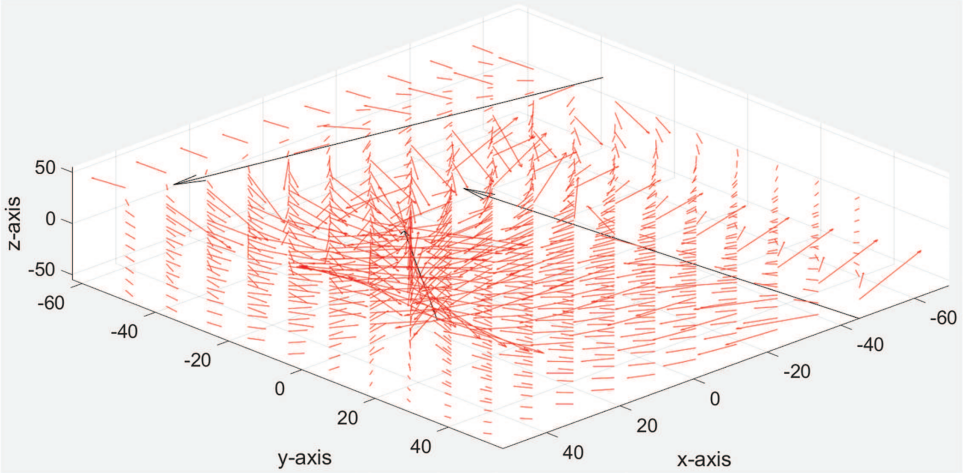

Figure 11: Three-dimensional graph of the resultant $\vec{\mathbf{E}}$ field for Case Study 3, showing a frontal view of quadrant 1

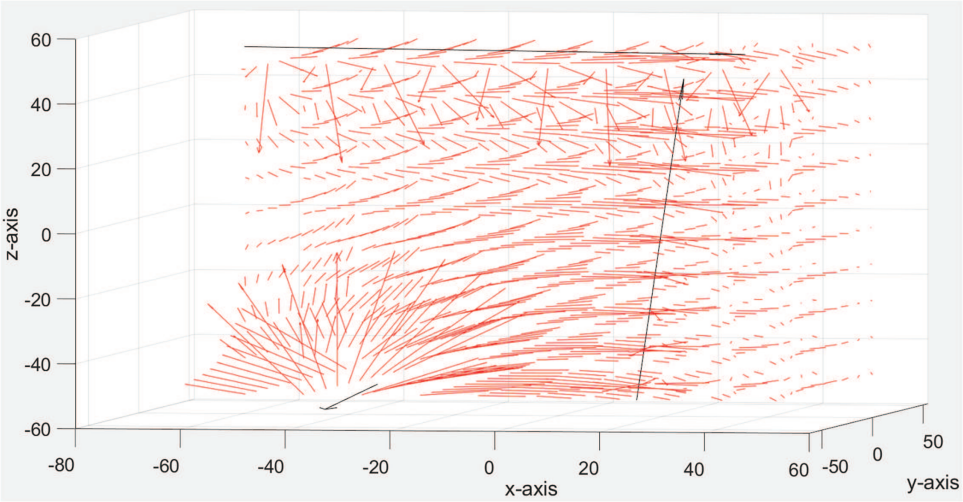

Figure 12: A third perspective showing the behavior of the $\vec{\mathbf{E}}$ field for Case Study 3

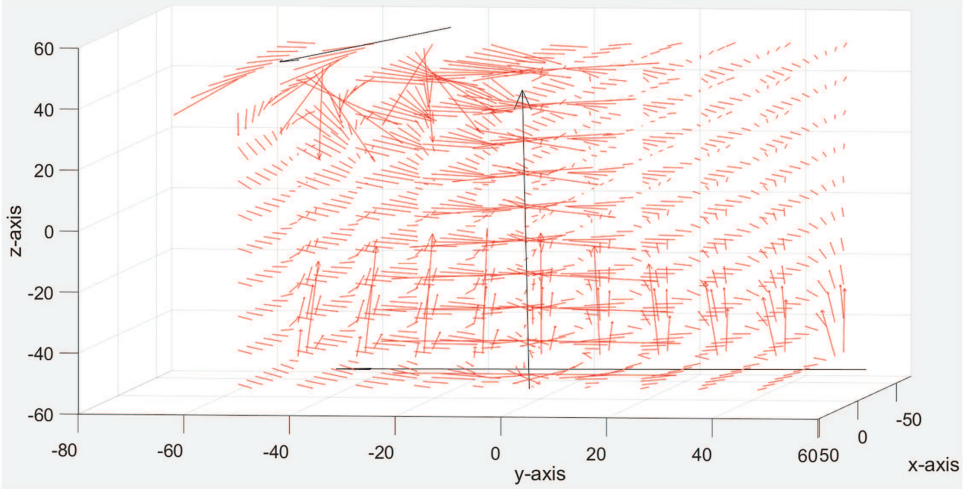

Figure 13: A fourth perspective showing the behavior of the $\vec{\mathbf{E}}$ field for Case Study 3

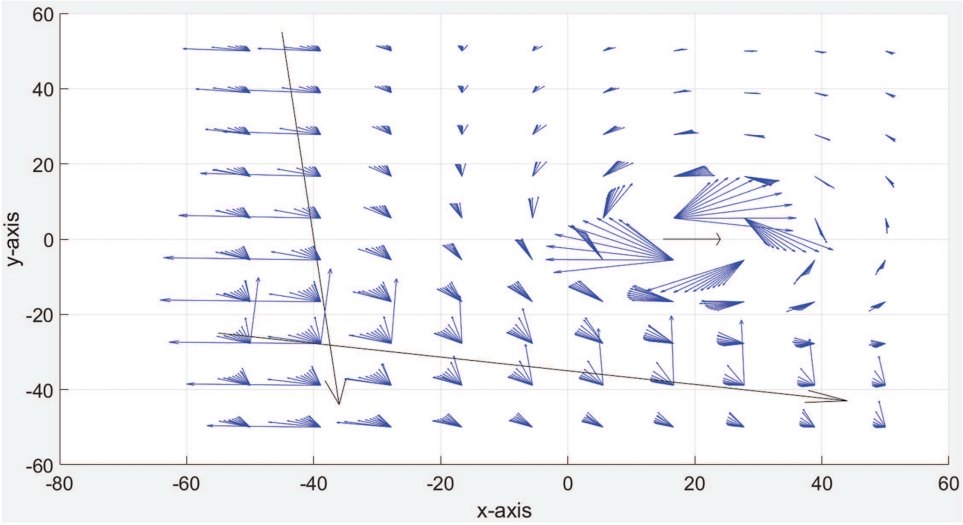

Figure 14: The $\vec{\mathbf{B}}$ field for Case Study 3 seen from the $+z$ axis (xy plane)

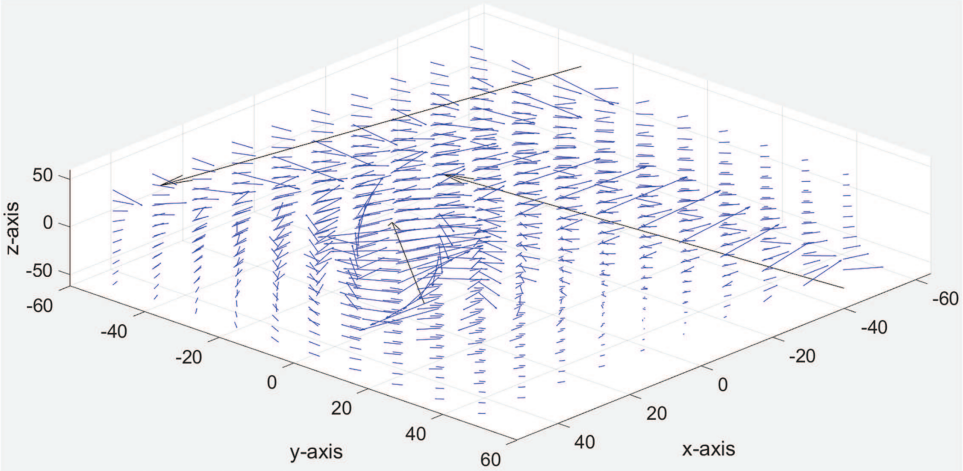

Figure 15: Three-dimensional graph of the resultant $\vec{\mathbf{B}}$ field for Case Study 3, showing a frontal view of quadrant 1

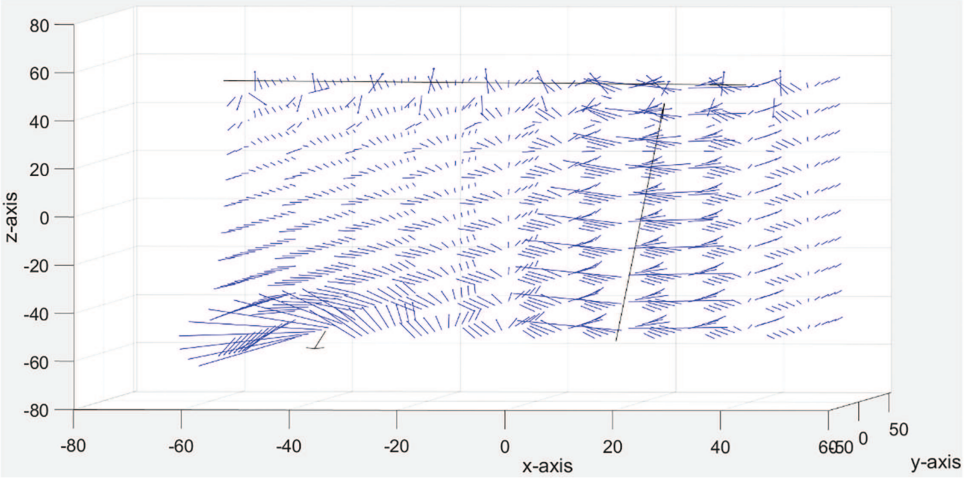

Figure 16: A third perspective showing the behavior of the $\vec{\mathbf{B}}$ field for Case Study 3

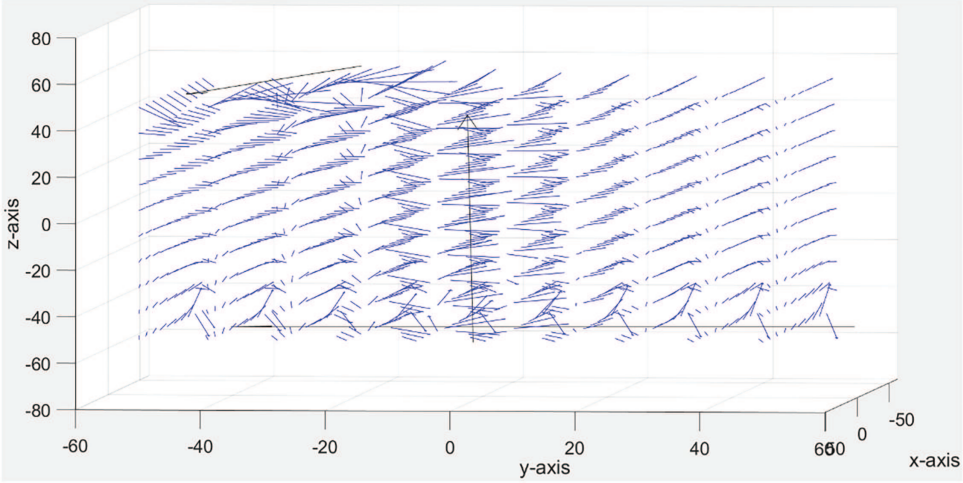

Figure 17: A fourth perspective showing the behavior of the $\vec{\mathbf{B}}$ field for Case Study 3

Figs. 10 and 14 show the plan views for the electric and magnetic fields, respectively, for this configuration of currents. Figs. 11 and 15 show three-dimensional views for those same fields. Figs. 12 and 16 show the behavior x vs. z for the electric and magnetic fields, respectively. Figs. 13 and 17 show the behavior y vs. z for the electric and magnetic fields, respectively.

Although it is quite difficult to obtain real behaviors of electric currents as arbitrary as those presented in case 3, in electrical fire laboratories it has been possible to observe behaviors of this type coming from dissipations in electrical power systems [39–42]. This illustrates the modeling benefits of this method, since otherwise, these results could only be obtained by separate models, and in many cases for specific configurations [43–47].

3.4 Case Study 4

We present a last case to show a practical and direct application that this model can have in the electromagnetic analysis of lines in real power systems. With the widespread use of overhead energy transmission lines, today it is common to see crossings of power transmission lines such as those shown in Fig. 18, where a crossing is observed between two high voltage lines 18a, a crossing between a high voltage line and one medium voltage line 18b, and a crossing between two medium voltage lines 18c.

Some of these situations occur near residential, commercial, and industrial facilities, where understanding electromagnetic compatibility is very important, such as hospital areas or technology centers.

(a)

(b)

(c)

Figure 18: Situations of power line crossings are shown on: (**a**) two high voltage lines; (**b**) high voltage and medium voltage line; and (**c**) two medium voltage lines

As an example, we present the analysis of a crossing between a three-phase high voltage line (115 kV) and a medium voltage line (13.5 kV), with the following specific characteristics. The three-phase medium voltage line carries a current of 100 amperes balanced and the three-phase high voltage line carries a current of 200 amperes balanced as shown in Table 1.

Table 1: Space points and description for 3 Ph-Lines 1 and 2 in the transmission system for case study 4

3 Ph-Line	$\boldsymbol{i}\,(\boldsymbol{t})_{(\boldsymbol{ijN})}$	Line description based on points $\boldsymbol{P}_{\boldsymbol{iN}}(\overline{\boldsymbol{x}},\overline{\boldsymbol{y}},\overline{\boldsymbol{z}})$ and $\boldsymbol{P}_{\boldsymbol{jN}}(\overline{\boldsymbol{x}},\overline{\boldsymbol{y}},\overline{\boldsymbol{z}})$
3 Ph-Line 1 MV	$i\,(t)_{(ab1)}$ $i\,(t)_{(cd1)}$	Passes through $P_{a1}(-2,-50,10)$ and $P_{b1}(-2,50,10)$ Passes through $P_{c1}(0,-50,10)$ and $P_{d1}(0,50,10)$

(Continued)

Table 1 (continued)

3 Ph-Line	$\boldsymbol{i\,(t)_{(ijN)}}$	Line description based on points $\boldsymbol{P_{iN}(\overline{x},\overline{y},\overline{z})}$ and $\boldsymbol{P_{jN}(\overline{x},\overline{y},\overline{z})}$
3 Ph-Line 2 HV	$i\,(t)_{(ef1)}$	Passes through $P_{e1}(2,-50,10)$ and $P_{f1}(2,50,10)$
	$i\,(t)_{(ab2)}$	Passes through $P_{a2}(-50,-2,15)$ and $P_{b2}(50,-2,15)$
	$i\,(t)_{(cd2)}$	Passes through $P_{c2}(-50,0,15)$ and $P_{d2}(50,0,15)$
	$i\,(t)_{(ef2)}$	Passes through $P_{e2}(-50,2,15)$ and $P_{f2}(50,2,15)$

Note that the nomenclature of the phases of each power line has been of the $i(t)_{(ijN)}$ style instead of the simple $i(t)_{(1)}$, $i(t)_{(2)}$, $i(t)_{(3)}$ style, in order to provide a direct relationship with the points $P_{iN}(\overline{x},\overline{y},\overline{z})$ and $P_{jN}(\overline{x},\overline{y},\overline{z})$ that demarcates and gives direction to each of the phase lines. To adequately characterize the electrostatic effect of the ground on the surface line charges (capacitance of transmission lines), we will use the image method [48,49] and define the negatives of the proposed lines, as imaginary lines below the ground level (that is, in negative z), in equal magnitudes and distances of $z = 0$, but negatives. These would be lines 3 and 4 mirroring lines 1 and 2, respectively, as shown in Table 2.

Table 2: Space points and description for 3 Ph-Lines 3 and 4 (mirrored lines) in the transmission system for case study 4

3 Ph-Line	$\boldsymbol{i\,(t)_{(ijN)}}$	Line description based on points $\boldsymbol{P_{iN}(\overline{x},\overline{y},\overline{z})}$ and $\boldsymbol{P_{jN}(\overline{x},\overline{y},\overline{z})}$
3 Ph-Line 3 MV img.	$i\,(t)_{(ab3)}$	Passes through $P_{a3}(-2,-50,-10)$ and $P_{b3}(-2,50,-10)$
	$i\,(t)_{(cd3)}$	Passes through $P_{c3}(0,-50,-10)$ and $P_{d3}(0,50,-10)$
	$i\,(t)_{(ef3)}$	Passes through $P_{e3}(2,-50,-10)$ and $P_{f3}(2,50,-10)$
3 Ph-Line 4 HV img.	$i\,(t)_{(ab4)}$	Passes through $P_{a4}(-50,-2,-15)$ and $P_{b4}(50,-2,-15)$
	$i\,(t)_{(cd4)}$	Passes through $P_{c4}(-50,0,-15)$ and $P_{d4}(50,0,-15)$
	$i\,(t)_{(ef4)}$	Passes through $P_{e2}(-50,2,-15)$ and $P_{f2}(50,2,-15)$

The general intensities of the three phases of the transmission set 1 are given by: $i(t)_{(ab1)} = 100cos\,(\omega t)$, $i(t)_{(cd1)} = 100cos\left(\omega t + \frac{120^\circ}{180^\circ}rad\right)$, and $i(t)_{(ef1)} = 100cos\left(\omega t + \frac{240^\circ}{180^\circ}rad\right)$.

The general intensities of the three phases of the transmission set 2 are given by: $i(t)_{(ab2)} = 200cos\,(\omega t)$, $i(t)_{(cd2)} = 200cos\left(\omega t + \frac{120^\circ}{180^\circ}rad\right)$, and $i(t)_{(ef2)} = 200cos\left(\omega t + \frac{240^\circ}{180^\circ}rad\right)$.

As defined, the sets of lines 3 and 4 for the ground effects are incorporated into the model, simply defining the negatives of the currents already presented in Euclidean locations reflected with respect to the plane located z = 0 (considered ground plane). The values of these imaginary currents would

be given by: $i(t)_{(ab3)} = -i(t)_{(ab1)}$, $i(t)_{(cd3)} = -i(t)_{(cd1)}$, $i(t)_{(ef3)} = -i(t)_{(ef1)}$, $i(t)_{(ab4)} = -i(t)_{(ab2)}$, $i(t)_{(cd4)} = -i(t)_{(cd2)}$, and $i(t)_{(ef4)} = -i(t)_{(ef2)}$. The Hertzian frequency of our system is 60 Hz, therefore the radiant frequency will be approximated to $\omega = 377$, and we can represent the system in phasor mode as used in case 3: $I_{(ab1)} = \frac{100}{\sqrt{2}}\angle 0°$, $I_{(cd1)} = \frac{100}{\sqrt{2}}\angle 120°$, $I_{(ef1)} = \frac{100}{\sqrt{2}}\angle 240°$, $I_{(ab2)} = \frac{200}{\sqrt{2}}\angle 0°$, $I_{(cd2)} = \frac{200}{\sqrt{2}}\angle 120°$, and $I_{(ef2)} = \frac{100}{\sqrt{2}}\angle 240°$. The imaginary currents reflected in sets 3 and 4 to model the ground effect would simply be the negatives already discussed.

Using Eqs. (6) and (7), along with typical values of equivalent capacitance and line voltage obtained from a SCADA system, the charge densities used for this case correspond to: $\lambda_1 = \left(0.23567 \times 10^{-6}\right) \frac{C}{m}$ for each of the lines of set 1, and $\lambda_2 = \left(0.35350 \times 10^{-6}\right) \frac{C}{m}$ for each of the lines of set 2. The dynamics of variation with time has been considered under the same parameter of variation of the currents, considering that the lines are balanced and the Maxwellian linkage is ideally fulfilled in the conducting medium. Imaginary densities to model the ground effect have been defined in sets 3 and 4, as: $\lambda_3 = -\lambda_1$ and $\lambda_4 = -\lambda_2$.

In this case, our model can be considered very complex as it handles a total of 12 electric current lines (of which we only require real information on 6), but with the methodology presented, all electromagnetic fields can be evaluated following Eqs. (12)–(20). The results of this case are widely shown in Figs. 19–23. In Fig. 19, we can see the described scheme, with the high voltage (HV) lines at level $z = 15$ (3 Ph-Line 2 of Table 1), the medium voltage (MV) lines at level $z = 10$ (3 Ph-Line 1 of Table 1), the ground level at $z = 0$ and the image lines of high and medium voltage below z (3 Ph-Lines 4 and 3 of Table 2, respectively). It is observable how in the electrical case, high voltage lines cause a greater impact on the electric field vectors close to medium voltage lines.

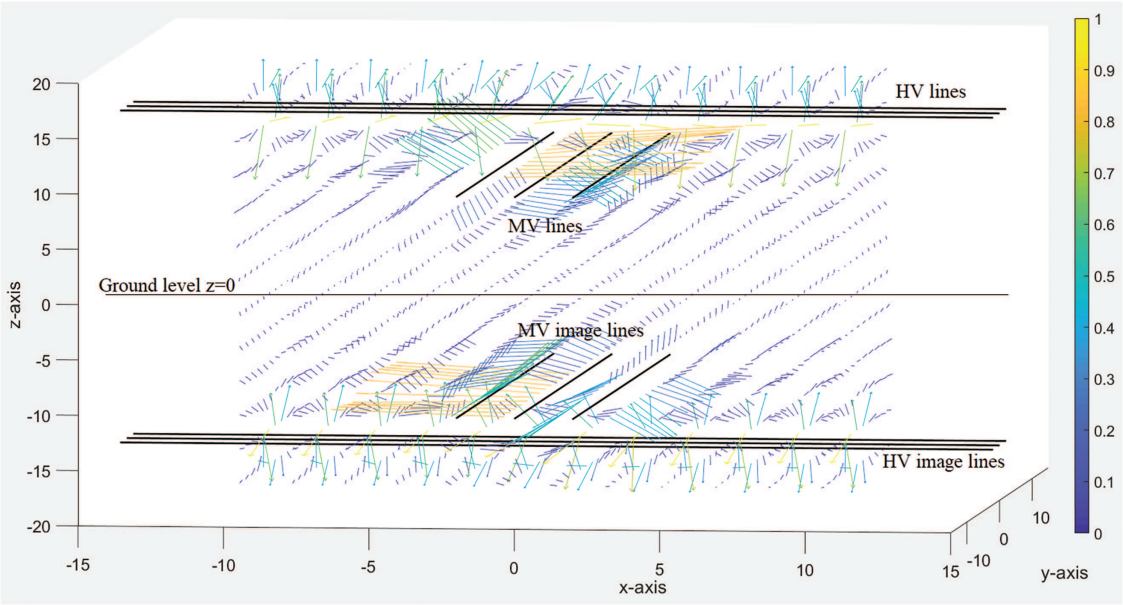

Figure 19: The results for electric field vectors of case 4 are shown, with the complete 12-line scheme. The normalized field intensity has been identified by color for greater detail. The influence of instantaneous phase imbalance and image line effects is visible in the asymmetries of the field

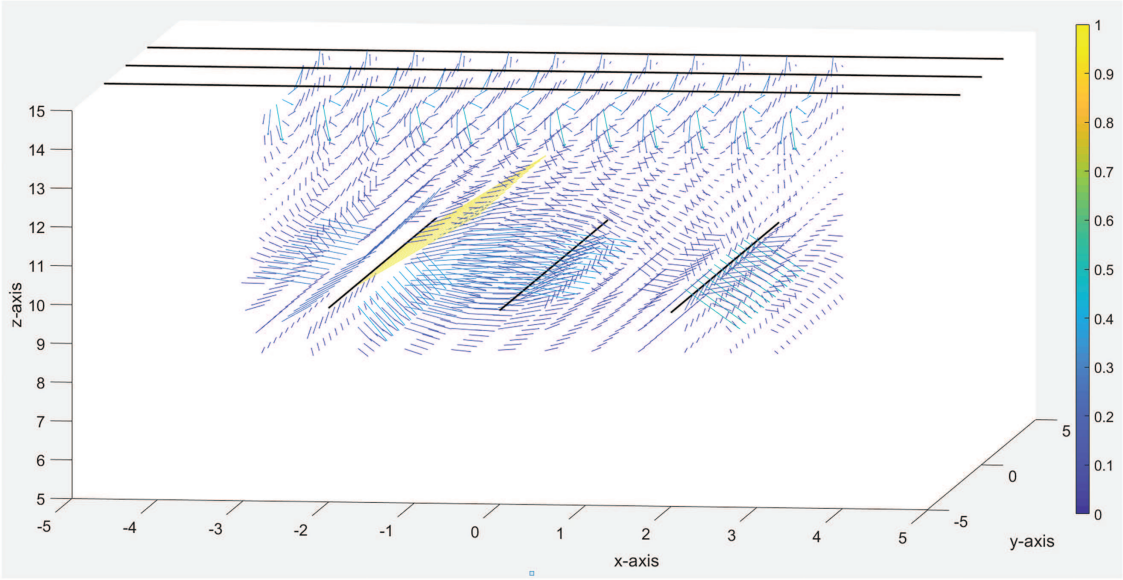

Figure 20: The results for electric field vectors of case 4 concentrating the calculation data only on the real lines. The normalized field intensity has been identified by color for greater detail. The influence of instantaneous phase imbalance is visible in the asymmetries of the field, especially near the crossing region

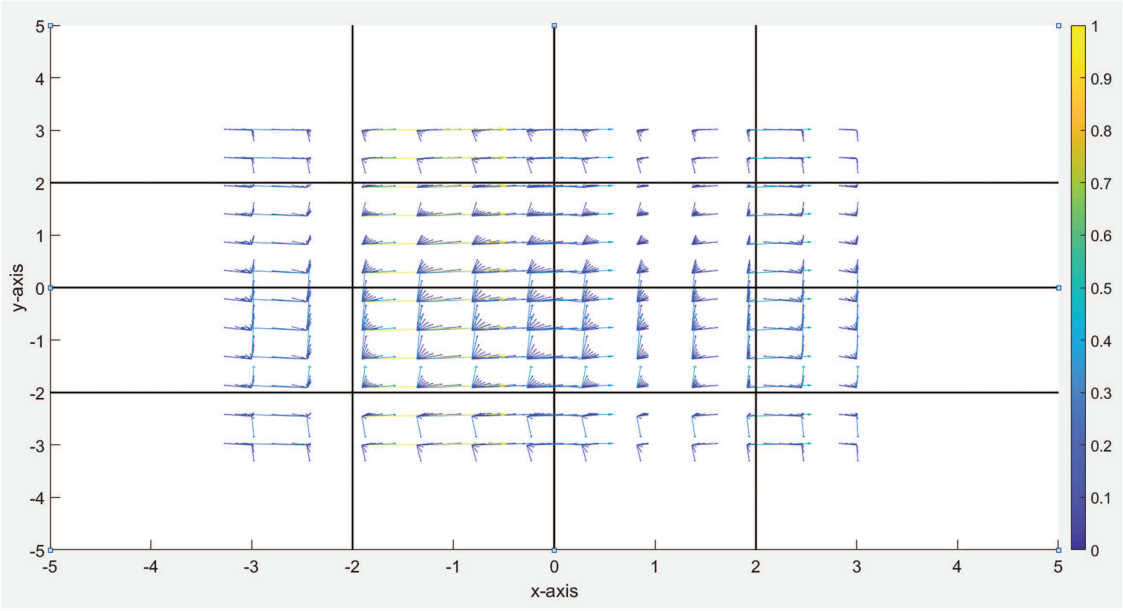

Figure 21: View of the magnetic field vectors from the $+z$ axis. The normalized field intensity has been identified by color for greater detail. The instantaneous phase imbalance is visible in the asymmetries of the field

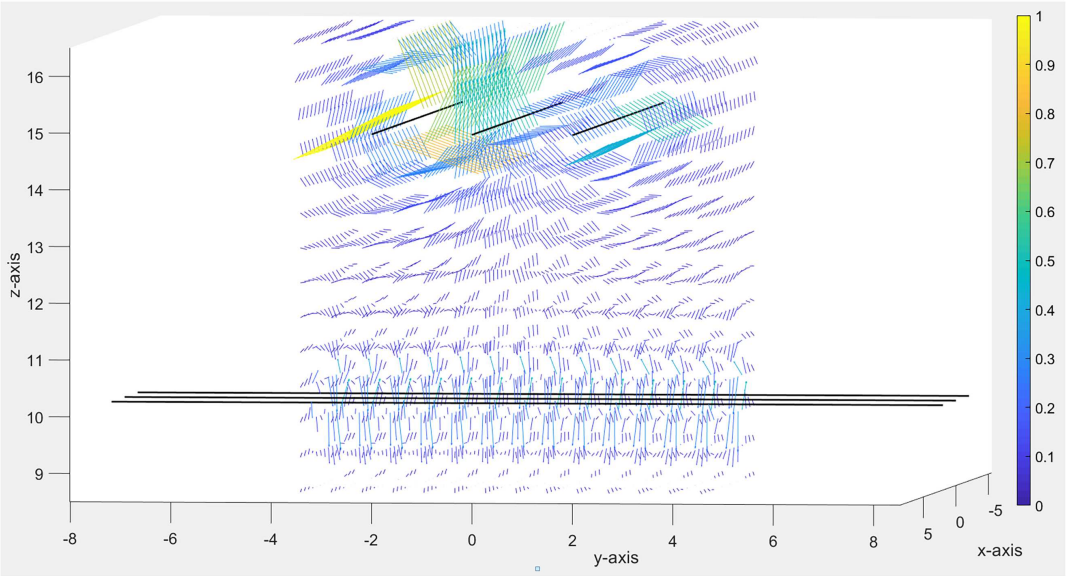

Figure 22: View of the magnetic fields, where the interaction and effect of the MV line (lower) on the HV line (upper) is noted. The normalized field intensity has been identified by color for greater detail. The influence of instantaneous phase imbalance is visible in the asymmetries of the field, especially near the crossing region

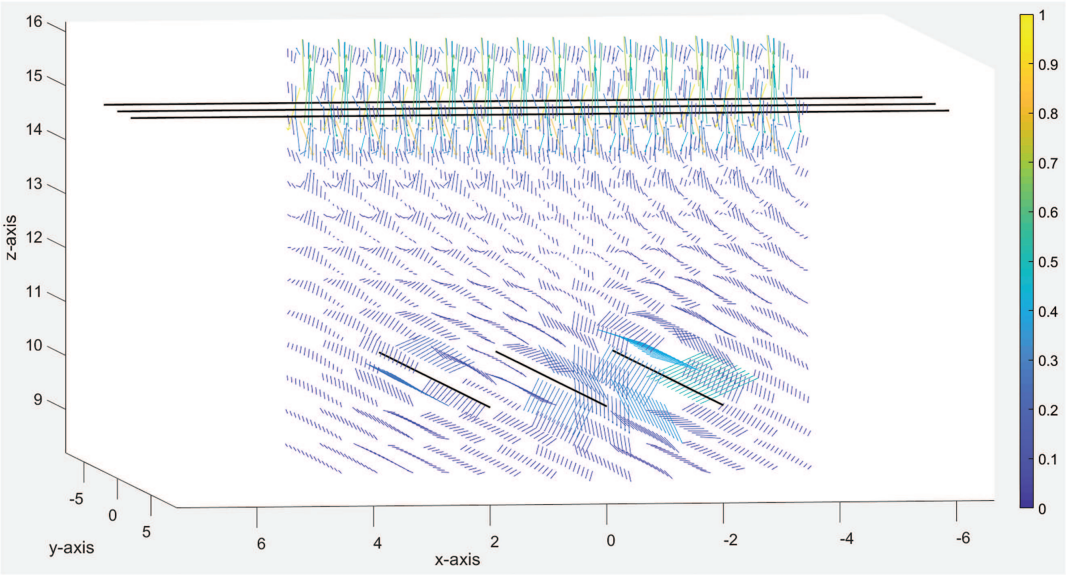

Figure 23: View of the magnetic fields, where the interaction and effect of the HV line (upper) on the MV line (lower) is noted. The normalized field intensity has been identified by color for greater detail. The influence of instantaneous phase imbalance is visible in the asymmetries of the field, especially near the crossing region

Fig. 20 details the electrical interaction described in greater detail, by dedicating all the calculation space to the volume existing between the HV and MV lines (over z). The curvature of electric fields

can also be observed in which the fields leaving line 1 seem to reach lines 2 and 3 of MV lines, due to the potential difference and the electrical phase difference.

The results of the magnetic field modeling for this case can be observed in Figs. 21–23. In Fig. 21, we can see a distribution of magnetic intensities that is not symmetrical, because the image has been taken considering an initial time $t = 0$ for the current phasors, a condition in which the instantaneous intensities of the second and third phases of both three-phase lines (HV and MV), are lower than the instantaneous intensity of the first phase.

In Figs. 22 and 23, we can see the circulation behavior of the magnetic fields around the conductors, where the interaction of the electric current intensities between the MV line and the HV line is noticeable, and is shown completely modeled.

The analysis of the electromagnetic field interactions in Case Study 4 highlights key aspects of power transmission line crossings, particularly regarding electromagnetic compatibility (EMC). In practical scenarios, the superposition of electric and magnetic fields from different voltage levels can influence induced voltages in nearby conductors, potentially affecting power quality and safety. One significant concern is the impact of high-voltage (HV) lines on medium-voltage (MV) infrastructure, as the increased electric field intensity near MV conductors may lead to enhanced corona discharge effects or insulation stress. Additionally, magnetic field interactions between the two systems could induce unwanted currents in adjacent infrastructure, such as grounding systems or nearby communication lines.

4 Comparison with Existing Modeling Techniques

To evaluate the performance of the proposed method against existing modeling techniques, a case study was designed with three infinite charged conductors positioned in Euclidean space as shown in Table 3:

Table 3: Description of electrical charges and currents used in the comparative case

$\boldsymbol{i(t)}_{(N)}$ source name	Line description based on points $\boldsymbol{P}_{iN}(\overline{x},\overline{y},\overline{z})$ and $\boldsymbol{P}_{jN}(\overline{x},\overline{y},\overline{z})$	Electrical current (A)	Electrical charge (μC/m)
$i\,(t)_{(1)}$	Passes through $P_{a1}(-1,0,0)$ and $P_{b1}(-1,0,1)$	100	0.100
$i\,(t)_{(2)}$	Passes through $P_{c2}(1,0,0)$ and $P_{d2}(1,0,1)$	50	0.050
$i\,(t)_{(3)}$	Passes through $P_{e3}(1,1,0)$ and $P_{f3}(1,1,1)$	25	0.025

Although this configuration is not symmetric, exact analytical solutions for the electric and magnetic fields at the origin can be obtained by superimposing individual solutions derived from Gauss's and Ampère's Laws. This allows a direct comparison with numerical methods without excessive mathematical complexity. The selected methods for comparison include: Finite Element Method Magnetics (FEMM) [50], ANSYS Maxwell 3D [51], and the method proposed in this article (Analytical Euclidean Method—AEM) implemented in MATLAB [31].

Figs. 24–29 present the results obtained. Figs. 24 and 25 show electric and magnetic field simulations using FEMM. Figs. 26 and 27 show electric and magnetic field simulations using ANSYS Maxwell 3D. Figs. 28 and 29 show simulation using the proposed method in MATLAB.

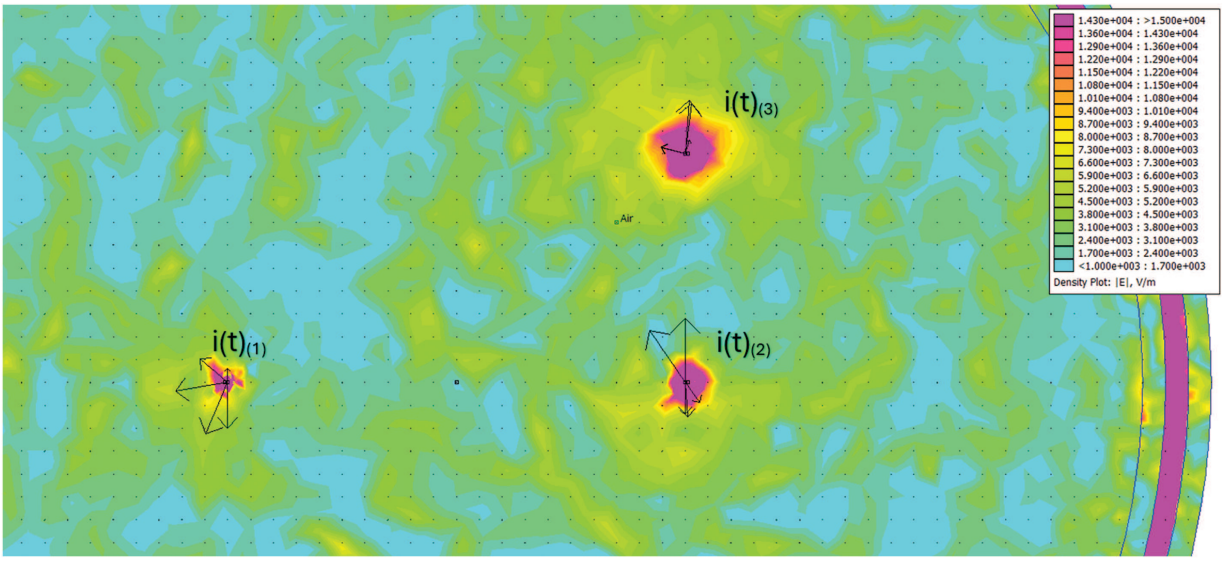

Figure 24: Result of the FEMM simulation of the electric field for the case described in Table 3

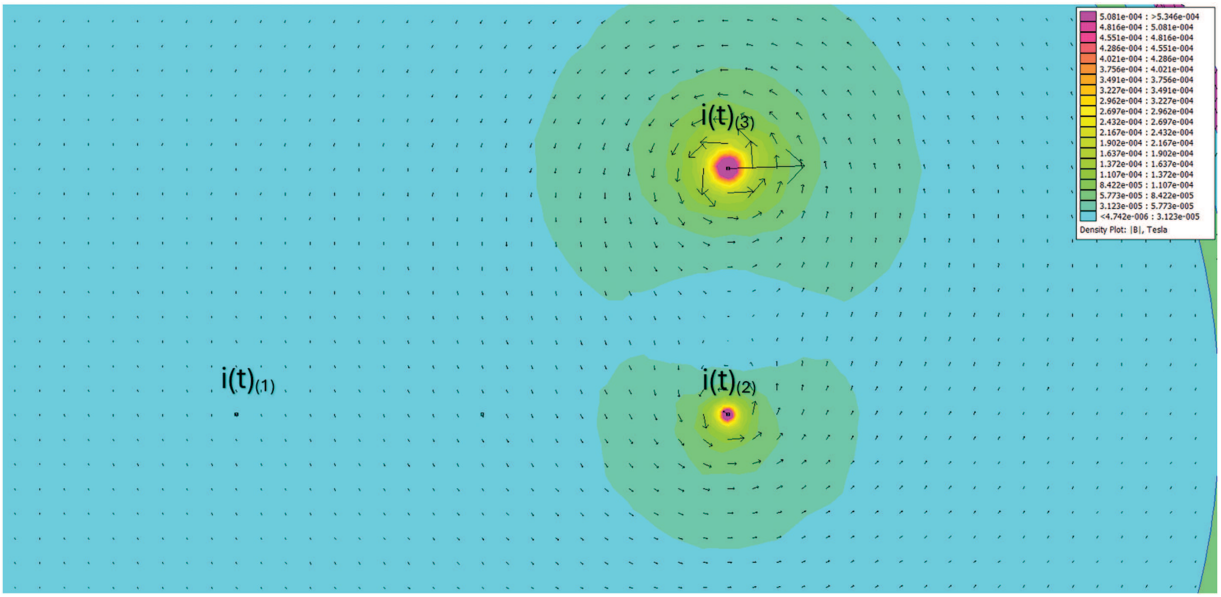

Figure 25: Result of the FEMM simulation of the magnetic field for the case described in Table 3

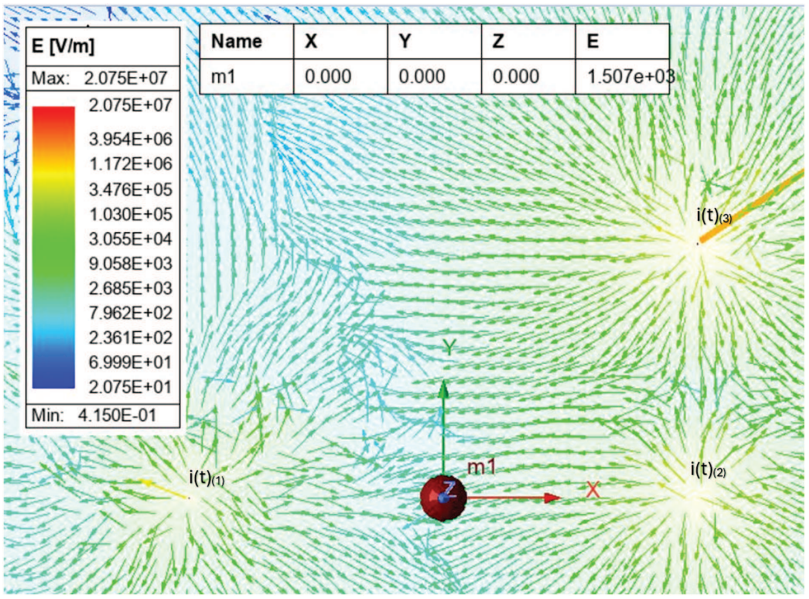

Figure 26: Result of the ANSYS Maxwell simulation of the electric field for the case described in Table 3

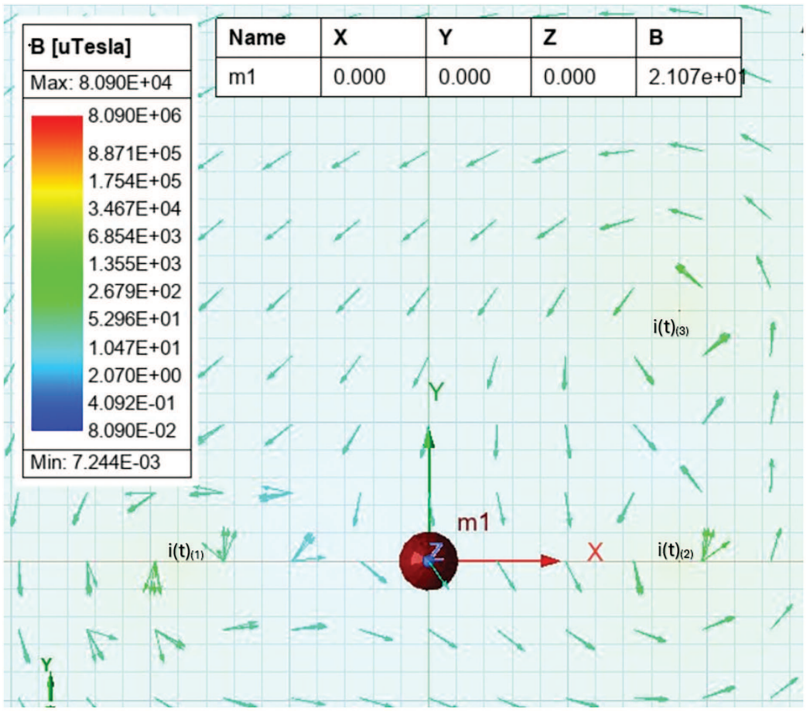

Figure 27: Result of the ANSYS Maxwell simulation of the magnetic field for the case described in Table 3

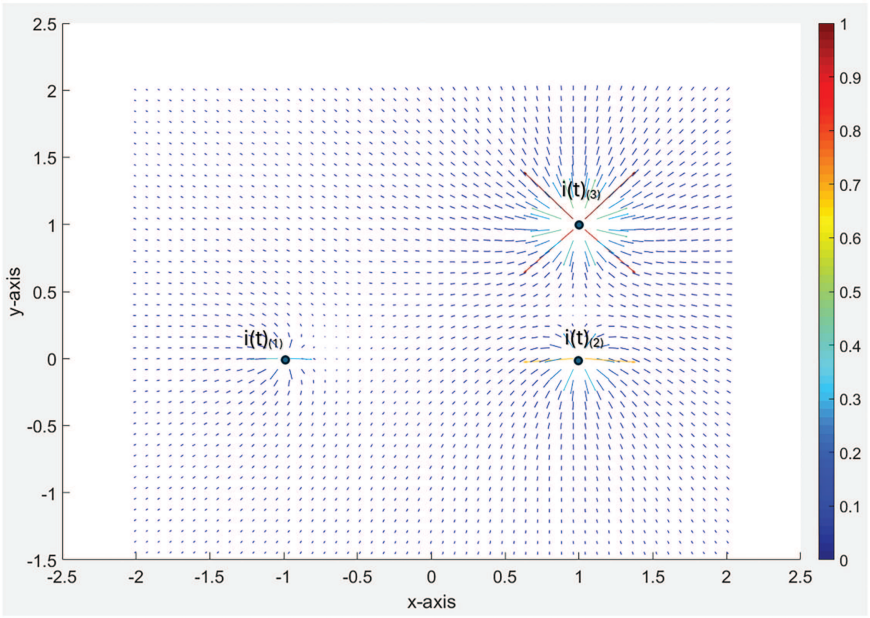

Figure 28: Result of electric field simulation with the proposed Euclidean Method for Multiple Conductors, for the case described in Table 3. The normalized field intensity has been identified by color

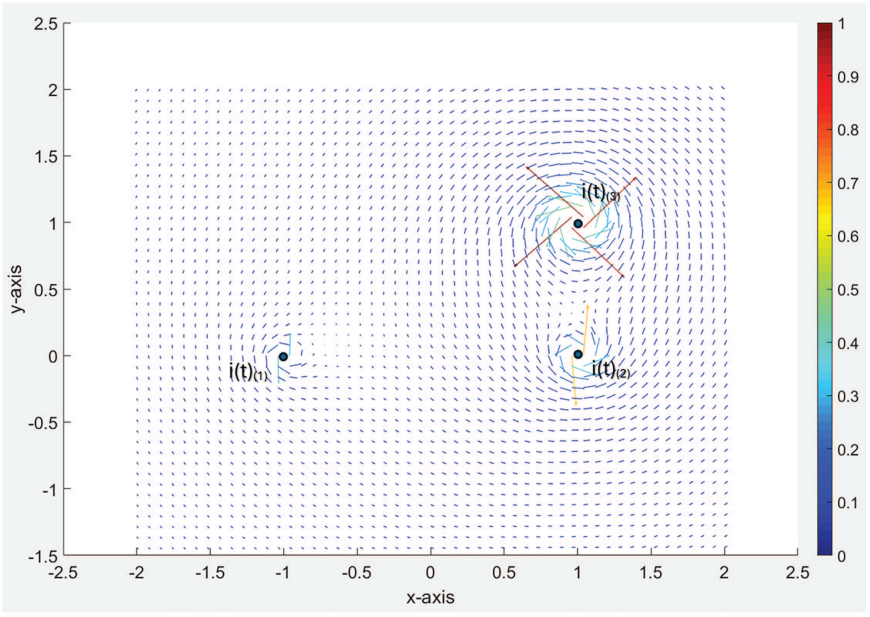

Figure 29: Result of magnetic field simulation with the proposed Euclidean Method for Multiple Conductors, for the case described in Table 3. The normalized field intensity has been identified by color

The formal analytical exact computation of electric and magnetic fields at the point $(x, y, z) = (0, 0, 0)$, assuming unitary relative permittivity and permeability, provides exact reference magnitudes

for this case: $\left|\vec{E}\right| = 450\sqrt{13}\left[\frac{V}{m}\right]$, and $\left|\vec{B}\right| = \frac{\sqrt{13}}{200000}[T]$. Using these values as benchmarks, the comparative results are summarized in Table 4.

Table 4: Comparative results of the modeling methods and tools in (x, y, z) = (0, 0, 0), for the case described in Table 3

Tool	Method	Calc. Nodes	$\left\|\vec{E}\right\|_{(0,0,0)}\left[\frac{V}{m}\right]$	$\left\|\vec{B}\right\|_{(0,0,0)}[T]$	%err E	%err B
Finite Element Method Magnetics (FEMM)	Finite element method	14,476	1446.12	2.0231E−05	10.87%	12.22%
ANSIS maxwell 3D	Finite element method	19,200	1.507E+03	2.1690E−05	7.12%	20.31%
CEM using analytical Euclidean method for multiple conductors (proposed)	Analytical Euclidean method	2601	1622.50	1.8028E−05	0.00%	0.00%

The results indicate that the proposed method provides an exact solution for this case study while also achieving a significant reduction in the number of computation nodes compared to finite element methods. This improved efficiency suggests that the approach may be advantageous in scenarios where minimizing computational resources is critical.

It is important to note that neither FEMM nor ANSYS Maxwell can define truly infinite charge elements, requiring spatial boundaries and domain discretization using the Finite Element Method (FEM). This represents a fundamental difference from the proposed method, which models current lines vectorially using only two reference points. Conventional finite element strategies divide the space into nodes that approximate the continuous field, a process that introduces error and lengthens computing time. Unlike FEM-based approaches, our method computes values directly and avoids these approximations. Additionally, it does not require mesh generation or a predefined computational space, significantly reducing the number of computation nodes while maintaining accuracy.

5 Discussion

This method obtains precise results for the electric and magnetic fields linked to any number of infinite lines of current single Euclidean space, regardless of their directions, in a direct and simple way. Previous engineering method could handle several current lines, but they only worked when the placement and number of the lines could fulfill symmetry requirements. By contrast, the method presented here does not depend on symmetry, nor does it have limitations on the number of current lines used.

The implications of this method extend widely across various areas of electrical engineering, as demonstrated in Case Study 4. Additionally, it is highly applicable in electronics and other fields where modeling electromagnetic fields in Euclidean spaces is essential, such as radiation analysis and electrical fire investigations. This method also holds significant potential in telecommunications,

considering that much of the electrical infrastructure used for power systems is also utilized for communication, whether underground or overhead. The compatibility of power and communication signals is an important issue due to the intensities and directions of the electromagnetic fields involved in the interacting systems, especially if the fields are created by power lines that could seriously affect the operation of systems with weaker signals. These systems can often be modeled as very long (quasi-infinite) current lines, but their directions in practical cases are very different, as can be seen in Fig. 30.

Figure 30: View of power and communications line systems in different directions, sharing the same space and infrastructure

The proposed method provides a straightforward approach to solving a wide range of practical engineering problems. Since it offers a general analytical solution for infinite current-carrying lines, its potential applications in electrical engineering are as extensive as those of traditional models based on Gauss's and Ampere's Laws. However, unlike these classical approaches, our method does not require symmetry assumptions. Although some existing Finite Element Method (FEM)-based tools can provide approximate solutions for this class of calculations involving very long linear elements, they are inherently limited by the requirement that field-generating source lines must be contained within their modeling space. As a result, applying these methods to extensively long conductors lead to significantly higher computational costs and increased approximation errors. These limitations arise from the necessity to discretize large spatial domains, which not only demands greater computational resources but also introduces numerical inaccuracies due to boundary truncation and interpolation effects.

Unlike Finite Element Method (FEM)-based solvers, such as FEMM and ANSYS Maxwell, which primarily compute scalar potentials at the nodes and derive electric and magnetic fields through numerical differentiation [50,51], the proposed method directly computes both electric and magnetic field vectors at each node. This eliminates the need for interpolation from element-based values, reducing numerical errors and improving accuracy. This direct computation also facilitates a more precise evaluation of field interactions.

The method is primarily designed for applications involving linear, homogeneous, and isotropic materials, as well as current-carrying conductors that can be approximated as infinite lines, such as overhead power distribution systems. It is also applicable to other types of long conductors in free space or embedded in isotropic materials, including communication lines, transmission cables, and grounded conductors. While this approach provides an exact analytical solution under these conditions, it may not be directly applicable to scenarios involving anisotropic materials, composite conductors, or complex boundary conditions. In such cases, the numerical methods such as the Finite Element

Method (FEM) [51] or Finite Difference Time Domain (FDTD) [52] are often required to account for material-dependent variations in electromagnetic field behavior [53]. Future work could explore potential extensions of this method to incorporate anisotropic media by modifying the governing equations to include material-dependent permittivity and permeability tensors.

6 Conclusions

With the high levels of supervision and control that exist today in the operation of electrical systems, due to the extensive development and integration of systems such as SCADA, we can indicate that the internal parameters of the lines are known with great precision. However, until now, achieving something similar with respect to the characterization of the electromagnetic fields external to the lines, has not been possible in a simple way, and these fields have the possibility of affecting other nearby systems. In this work, a method has been presented that greatly simplifies the practical characterization of the described fields, so that it can be used at an engineering level in the design or inspection of these systems.

We have described a precise and simple analytical method to solve the magnetic and electric fields due to multiple infinite current-carrying conductors in a single Euclidean space, regardless of the directions followed by the currents. This method was tested with 4 study cases: case 1 had a single line of current, allowing the validation of results, since the behavior is already well known in Classic Electromagnetics. Case Study 2, on the other hand, consisted of two parallel lines with spatial symmetry. Case Study 3 presented a more complicated scenario with three infinite linear conductors spatially oriented in various directions and carrying currents of different intensities, showing the simplicity with which electromagnetic fields can be modeled using this method, which is kept simple, only uses a single reference frame for all data and results, does not require the use of rotated or translated matrices and is not limited to any of the line symmetry criteria commonly found in other engineering methods for these purposes. Finally, Case Study 4 showed the use of the method in a very common case found in the electrical power systems of our days, the crossing of two three-phase power lines, whose detailed electromagnetic modeling has been acquired with simplicity thanks to the direct application of this method.

The proposed method has also been compared with well-established solution techniques and tools such as ANSYS Maxwell and FEMM, demonstrating superior accuracy while requiring significantly fewer computational nodes. This efficiency stems from the direct calculation of electric and magnetic field vectors at each point, eliminating the need for extensive meshing and numerical interpolation, which are inherent to finite element-based methods.

The proposed method has direct modeling applications in electrical, electronic, and communications engineering; as well as in a wide variety of situations and industrial applications in which there are electric current lines that can be modeled as quasi-infinite.

Acknowledgement: The authors thank Eng. Esteban Rua for his support in the comparative modeling of this study.

Funding Statement: This research was funded by SENACYT-Panamá under grant FID23-017 of Public Call for R&D Promotion (FID) 2023 awarded to D.C., and the SNI program of the National Secretariat of Science, Technology and Innovation (https://www.senacyt.gob.pa/, accessed on 01 June 2025). We also appreciate the contribution of CEMCIT-AIP (https://cemcit.org.pa/, accessed on 01 June 2025) in accordance with the financial management of the project.

Author Contributions: The authors confirm contribution to the paper as follows: Conceptualization, Dorindo Cardenas; data curation, Dorindo Cardenas, methodology, Dorindo Cardenas; formal analysis, Dorindo Cardenas; funding acquisition, Dorindo Cardenas, Sherlie Portugal, and Alejandro Von Chong; investigation, Dorindo Cardenas, Sherlie Portugal, and Alejandro Von Chong; project administration, Dorindo Cardenas; resources, Dorindo Cardenas, Sherlie Portugal, and Alejandro Von Chong; software, Dorindo Cardenas and Alejandro Von Chong; supervision, Dorindo Cardenas; validation, Dorindo Cardenas, Sherlie Portugal, and Alejandro Von Chong; writing—original draft, Dorindo Cardenas, Sherlie Portugal, and Alejandro Von Chong; writing—review and editing, Dorindo Cardenas, Sherlie Portugal, and Alejandro Von Chong. All authors reviewed the results and approved the final version of the manuscript.

Availability of Data and Materials: The data that support the findings of this study are available from the corresponding author, Dorindo Cardenas, upon reasonable request.

Ethics Approval: Not applicable.

Conflicts of Interest: The authors declare no conflicts of interest to report regarding the present study.

Appendix A

This section provides the complete MATLAB code used for data acquisition, field computation, and visualization of the electric and magnetic fields, based on the proposed model applied to a three-phase power line case.

```
% MATLAB CODE FOR CALCULATION OF E & B FIELDS OF A 3PHASE POWER LINE WITH ARB DIRECTIONS
clc
clear all
close all
disp('This program calculates the E and B fields for THREE infinite lines with currents Iab, Icd and Ief respectively')
format long

%———CHARGE DEFINITIONS———-
%3phase line

disp('POINTS FOR FIRST 3-PHASE LINE')

Iab1 = input('Enter the value of electrical current in Amps for line "ab1":')

lab1 = input('Enter the linear electrical free charge in micro-Coul/m for line "ab1":')
lab1 = lab1/1000000

Icd1 = input('Enter the value of electrical current in Amps for line "cd1":')
```

```
lcd1 = input('Enter the linear electrical free charge in micro-Coul/m for line "cd1":')
lcd1 = lcd1/1000000

Ief1 = input('Enter the value of electrical current in Amps for line "ef1":')

lef1 = input('Enter the linear electrical free charge in micro-Coul/m for line "ef1":')
lef1 = lef1/1000000

disp('Now you have to select two points Pa1(xa1,ya1,za1) and Pb1(xb1,yb1,zb1) to
describe your infinite line for Iab1 - PaPb1')
xa1 = input('Enter xa1 location of your Pa1 point:')
ya1 = input('Enter ya1 location of your Pa1 point:')
za1 = input('Enter za1 location of your Pa1 point:')
xb1 = input('Enter xb1 location of your Pb1 point:')
yb1 = input('Enter yb1 location of your Pb1 point:')
zb1 = input('Enter zb1 location of your Pb1 point:')

Pa1 = [xa1, ya1, za1]
Pb1 = [xb1, yb1, zb1]

PaPb1 = [(xb1-xa1), (yb1-ya1), (zb1-za1)]

uiab1 = [(xb1-xa1), (yb1-ya1), (zb1-za1)]/sqrt((xb1-xa1)
^2 + (yb1-ya1)^2 + (zb1-za1)^2)

disp('Now you have to select two points Pc1(xc1,yc1,zc1) and Pd1(xd1,yd1,zd1) to
describe your infinite line for Icd1 - PcPd1')
xc1 = input('Enter xc1 location of your Pc1 point:')
yc1 = input('Enter yc1 location of your Pc1 point:')
zc1 = input('Enter zc1 location of your Pc1 point:')
xd1 = input('Enter xd1 location of your Pd1 point:')
yd1 = input('Enter yd1 location of your Pd1 point:')
zd1 = input('Enter zd1 location of your Pd1 point:')

Pc1 = [xc1, yc1, zc1]
Pd1 = [xd1, yd1, zd1]

PcPd1 = [(xd1-xc1), (yd1-yc1), (zd1-zc1)]

uicd1 = PcPd1/norm(PcPd1)
```

```
disp('Now you have to select two points Pe1(xe1,ye1,ze1) and Pf1(xf1,yf1,zf1) to
describe your infinite line for Ief1 - PePf1')
xe1 = input('Enter xe1 location of your Pe1 point:')
ye1 = input('Enter ye1 location of your Pe1 point:')
ze1 = input('Enter ze1 location of your Pe1 point:')
xf1 = input('Enter xf1 location of your Pf1 point:')
yf1 = input('Enter yf1 location of your Pf1 point:')
zf1 = input('Enter zf1 location of your Pf1 point:')

Pe1 = [xe1, ye1, ze1]
Pf1 = [xf1, yf1, zf1]

PePf1 = [(xf1-xe1), (yf1-ye1), (zf1-ze1)]

uief1 = PePf1/norm(PePf1)
%------media definition----------

er = input('Enter the relative electrical permitivity of media:')

ur = input('Enter the relative magnetic permeability of media:')

BBbust = input('Enter the level of boosting (factor 0.1 - 1) that you want for graph B
over E:')

%-----interest points definition--------
xmin = input('Enter xmin location of your euclidean space:')
xmax = input('Enter xmax location of your euclidean space:')
ymin = input('Enter ymin location of your euclidean space:')
ymax = input('Enter ymax location of your euclidean space:')
zmin = input('Enter zmin location of your euclidean space:')
zmax = input('Enter zmax location of your euclidean space:')

PointDivX = input('Enter the quantity of divisions for X linear space:')
PointDivY = input('Enter the quantity of divisions for Y linear space:')
PointDivZ = input('Enter the quantity of divisions for Z linear space:')

xij = linspace(xmin,xmax,PointDivX)
yij = linspace(ymin,ymax,PointDivY)
zij = linspace(zmin,zmax,PointDivZ)
xi=1 %initializing x points generator
```

```
yi=1 %initializing y points generator
zi=1 %initializing z points generator
Pi = [xij(xi), yij(yi), zij(zi)]

while zi<(PointDivZ+0.5)

while yi<(PointDivY+0.5)

while xi<(PointDivX+0.5)

  disp(Pi)

%CALCULATIONS FOR FIELDS BEACUSE OF CURRENT Iab1
    disp('CALCULATIONS FOR FIELDS BECASE OF CURRENT Iab1')

    PaPi1 = [(Pi(1)-xa1), (Pi(2)-ya1), (Pi(3)-za1)]

    disp('The vector rphiab1')

    rphiab1 = cross(uiab1,PaPi1) %1st cross product

    disp('The vector roab1')

    roab1 = cross(rphiab1,uiab1) %2nd cross product

    disp('Unit vectors for Eab1 and Bab1')

    disp('Unit vector for Eab1:')
    uroab1 = roab1/norm(roab1)

    disp('Unit vector for Bab1:')
    urphiab1 = rphiab1/norm(rphiab1)

    disp('Final Vectors Eab1 and Bab1')

    disp('Final Electrical Field Vector Eab1')
    Eab1 = (2*9*10^9*lab1/(er*norm(roab1)))*uroab1

    disp('Final Magnetic Field Vector Bab1')
    Bab1 = (2*1*10^-7*Iab1*ur/norm(rphiab1))*urphiab1
```

```
%CALCULATIONS FOR FIELDS BEACUSE OF CURRENT Icd1
disp('CALCULATIONS FOR FIELDS BECAUSE OF CURRENT Icd1')

PcPi1 = [(Pi(1)-xc1), (Pi(2)-yc1), (Pi(3)-zc1)]

disp('The vector rphicd1')

rphicd1 = cross(uicd1,PcPi1) %1st cross product

disp('The vector rocd1')

rocd1 = cross(rphicd1,uicd1) %1nd cross product
disp('Unit vectors for Ecd1 and Bcd1')

disp('Unit vector for Ecd1:')
urocd1 = rocd1/norm(rocd1)

disp('Unit vector for Bcd1:')
urphicd1 = rphicd1/norm(rphicd1)

disp('Final Vectors Ecd1 and Bcd1')

disp('Final Electrical Field Vector Ecd1')
Ecd1 = (2*9*10^9*lcd1/(er*norm(rocd1)))*urocd1

disp('Final Magnetic Field Vector Bcd1')
Bcd1 = (2*1*10^-7*Icd1*ur/norm(rphicd1))*urphicd1

%CALCULATIONS FOR FIELDS BEACUSE OF CURRENT Ief
disp('CALCULATIONS FOR FIELDS BECASE OF CURRENT Ief1')

PePi1 = [(Pi(1)-xe1), (Pi(2)-ye1), (Pi(3)-ze1)]

disp('The vector rphief1')

rphief1 = cross(uief1,PePi1) %1st cross product

disp('The vector roef1')
```

```
roef1 = cross(rphief1,uief1) %2nd cross product

disp('Unit vectors for Eef1 and Bef1')

disp('Unit vector for Eef1:')
uroef1 = roef1/norm(roef1)

disp('Unit vector for Bef1:')
urphief1 = rphief1/norm(rphief1)

disp('Final Vectors Eef1 and Bef1')
disp('Final Electrical Field Vector Eef1')
Eef1 = (2*9*10^9*lef1/(er*norm(roef1)))*uroef1

disp('Final Magnetic Field Vector Bef1')
Bef1 = (2*1*10^-7*Ief1*ur/norm(rphief1))*urphief1

%Graphical representation
Edownab1 = 10^-3*Eab1   %10^-x only for graph scaling

hold on
Bbustab1 = BBbust*10^6*Bab1 %10^-x only for graph scaling

Lab1=10^0*PaPb1   %10^-x only for graph scaling

quiver3(Pa1(1), Pa1(2), Pa1(3), Lab1(1), Lab1(2), Lab1(3),'k')
xlabel('x-axis')
ylabel('y-axis')
zlabel('z-axis')
title('Representation of Etot(red), and Btot(blue) vectors, for Ijk(black)
currents')
grid on


Edowncd1 = 10^-3*Ecd1   %10^-x only for graph scaling

Bbustcd1 = BBbust*10^6*Bcd1 %10^-x only for graph scaling

Lcd1=10^0*PcPd1   %10^-x only for graph scaling

quiver3(Pc1(1), Pc1(2), Pc1(3), Lcd1(1), Lcd1(2), Lcd1(3),'k')
```

```
    Edownef1 = 10^-3*Eef1   %10^-x only for graph scaling

    Bbustef1 = BBbust*10^6*Bef1 %10^-x only for graph scaling

    Lef1=10^0*PePf1   %10^-x only for graph scaling
    quiver3(Pe1(1), Pe1(2), Pe1(3), Lef1(1), Lef1(2), Lef1(3),'k')

    Etot1 = Eab1+Ecd1+Eef1
    Btot1 = Bab1+Bcd1+Bef1
    %TOTAL FIELDS GRAPH

    Edowntot = Edownab1+Edowncd1+Edownef1
    quiver3(Pi(1), Pi(2), Pi(3), Edowntot(1), Edowntot(2), Edowntot(3),'r')
    hold on
    Bbusttot = Bbustab1+Bbustcd1+Bbustef1
    quiver3(Pi(1), Pi(2), Pi(3), Bbusttot(1), Bbusttot(2), Bbusttot(3),'b')


    xi = xi+1

    if xi>PointDivX
        break
    end

    Pi = [xij(xi), yij(yi), zij(zi)]

end

xi = 1 %reset xi of second round for yi=2 or greater

yi = yi + 1

if yi>PointDivY
        break
    end

Pi = [xij(xi), yij(yi), zij(zi)]
```

```
end

yi = 1 %reset yi of second round for zi=2 or greater

zi = zi + 1

if zi>PointDivZ
       break
   end

Pi = [xij(xi), yij(yi), zij(zi)]

end
```

References

1. Maxwell JC. A dynamical theory of the electromagnetic field. Phil Trans R Soc. 1865;155:459–512. doi:10.1098/rstl.1865.0008.
2. He G, Hao Y, Xie Y. The multi-station fusion-based radiation source localization method based on spectrum energy. Sensors. 2025;25(5):1339. doi:10.3390/s25051339.
3. Hu Y, Li C, Yang J. Research on electromagnetic wave propagation characteristics of multi-source partial discharge in cable intermediate joints. In: 2022 4th International Conference on Smart Power & Internet Energy Systems (SPIES); 2022 Dec 9–12; Beijing, China. p. 475–80. doi:10.1109/SPIES55999.2022.10081970.
4. Spitzer K. Electromagnetic modeling using adaptive grids-error estimation and geometry representation. Surv Geophys. 2024;45(1):277–314. doi:10.1007/s10712-023-09794-9.
5. Bao Y, Song J. Analysis of electromagnetic non-destructive evaluation modelling using Stratton-Chu formulation-based fast algorithm. Philos Trans A Math Phys Eng Sci. 2020;378(2182):20190583. doi:10.1098/rsta.2019.0583.
6. Sadiku M. Elements of electromagnetics. New York, NY, USA: Oxford University Press; 2018.
7. Cardenas D. Apuntes de Teoría Electromagnética. 2nd ed. Orlando, FL, USA: Kindle Direct Publishing; 2021.
8. Daniele V, Gilli M, Pignari S. EMC prediction model of a single wire transmission line crossing a circular aperture in a planar screen. IEEE Trans Electromagn Compat. 1996;38(2):117–26. doi:10.1109/15.494614.
9. Tashiro D, Hisakado T, Matsushima T, Wada O. Single-conductor transmission line model incorporating radiation reaction. IEEE Trans Electromagn Compat. 2021;63(4):1065–77. doi:10.1109/temc.2020.3041468.
10. Iñiguez de la Torre JI, García Flores A, Muñoz Muñoz JM, De Francisco Garrido C. Problemas de Electrodinámica Clásica. Salamanca, Spain: Ediciones Universidad de Salamanca; 2018.
11. Bhattacharya K, Mukhopadhyay S. Introduction to advanced electrodynamics. 1st ed. Singapore: Springer; 2022. doi:10.1007/978-981-16-7802-8.
12. Brandão Faria JA, Machado VM, Van Dommelen D. Comparison of zeroth-order and harmonic expansion calculation of the electrostatic parameters of three-conductor bundles. Electr Power Syst Res. 2011;81(2):488–94. doi:10.1016/j.epsr.2010.10.016.

13. Vilachá C, Otero AF, Moreira JC, Miguez E. EMF mitigation in the vicinity of a overhead power line. In: 2012 11th International Conference on Environment and Electrical Engineering; 2012 May 18–25; Venice, Italy. p. 308–12.
14. Guan H, Qian H, Kong H, Wang X, Fang F, Hu G. Simulation calculation for total electric field of three-phase power cable. In: 2016 IEEE International Conference on High Voltage Engineering and Application (ICHVE); 2016 Sep 19–22; Chengdu, China. doi:10.1109/ICHVE.2016.7800883.
15. National Fire Protection Association. National electrical code—NFPA 70. Quincy, MA, USA: NFPA; 2023.
16. IEC 60364. Electrical installations for buildings. Geneva, Switzerland: International Electrotechnical Commission; 2009.
17. Miceli M, Carvelli V, Drissi-Habti M. Modelling electro-mechanical behaviour of an XLPE insulation layer for hi-voltage composite power cables: effect of voids on onset of coalescence. Energies. 2023;16(12):4620. doi:10.3390/en16124620.
18. Yang X, Wang Z, Li J, Wu M, Wang G, Gao X, et al. Research on the carrier characteristics of power cables considering the aging status of insulation and semiconducting layers. Energies. 2024;17(22):5655. doi:10.3390/en17225655.
19. Pan L, Luo Y, Wang X, Lei D, Wang J, Zhang H, et al. Simulation research on the effects of air gaps and ambient temperature on a 27.5 kV power cable. Appl Sci. 2025;15(3):1028. doi:10.3390/app15031028.
20. Ahmad S, Rizvi ZH, Wuttke F. Unveiling soil thermal behavior under ultra-high voltage power cable operations. Sci Rep. 2025;15(1):7315. doi:10.1038/s41598-025-91831-1.
21. Acosta J, Amortegui F, Escobar A, Leon L, Rivera S. Design and implementation of prototype for XLPE cable aging test. Rev Int Métodos Numér Cálc Diseño Ing. 2020;36(3):35. doi:10.23967/j.rimni.2020.07.002.
22. Kusic GL, Garrison DL. Measurement of transmission line parameters from SCADA data. In: IEEE PES Power Systems Conference and Exposition 2004; 2004 Oct 10–13; New York, NY, USA. p. 440–5. doi:10.1109/PSCE.2004.1397479.
23. Taksana R, Romphochai S, Bhumkittipich K, Mithulananthan N. Design of power transformer fault detection of SCADA alarm using fault tree analysis, smooth Holtz-Winters, and L-BFGS for smart utility control centers. IEEE Access. 2024;12(1):116202–324. doi:10.1109/ACCESS.2024.3446804.
24. Wang Y, Xu W, Shen J. Online tracking of transmission-line parameters using SCADA data. IEEE Trans Power Deliv. 2016;31(2):674–82. doi:10.1109/TPWRD.2015.2474699.
25. Radwan RM, Mahdy AM, Abdel-Salam M, Samy MM. Electric field mitigation under extra high voltage power lines. IEEE Trans Dielectr Electr Insul. 2013;20(1):54–62. doi:10.1109/TDEI.2013.6451341.
26. Righini D, Passerini F, Tonello AM. Modeling transmission and radiation effects when exploiting power line networks for communication. IEEE Trans Electromagn Compat. 2018;60(1):59–67. doi:10.1109/TEMC.2017.2728370.
27. Challita U, Saad W, Bettstetter C. Interference management for cellular-connected UAVs: a deep reinforcement learning approach. IEEE Trans Wirel Commun. 2019;18(4):2125–40. doi:10.1109/TWC.2019.2900035.
28. Kaaya J, Anael S. Review on electromagnetic interference and compatibility in aeronautical radio communications systems—Tanzania case study. J Inf Eng Appl. 2014;4:93–102.
29. Wisaratapong T, Pechaksorn N. Effects of electromagnetic interference produced by smartphones on patients with permanent pacemakers (EMS-PPM study). Eur Heart J. 2022;43:ehac544.650. doi:10.1093/eurheartj/ehac544.650.
30. Razek A. Biological and medical disturbances due to exposure to fields emitted by electromagnetic energy devices—a review. Energies. 2022;15(12):4455. doi:10.3390/en15124455.
31. MATLAB. MathWorks [Internet]. [cited 2021 Feb 16]. Available from: https://www.mathworks.com/products/matlab.html.
32. Roulet B, Saint Jean M. Image charges revisited: beyond classical electrostatics. Am J Phys. 2000;68(4):319–24. doi:10.1119/1.19433.

33. Cardenas DE. Phantom impedances as an option to solve 3D symmetrical circuit arrangements. IEEE Lat Am Trans. 2018;16(1):155–62. doi:10.1109/TLA.2018.8291468.
34. van der Holst JJM, Uijttewaal MA, Ramachandhran B, Coehoorn R, Bobbert PA, de Wijs GA, et al. Modeling and analysis of the three-dimensional current density in sandwich-type single-carrier devices of disordered organic semiconductors. Phys Rev B. 2009;79(8):085203. doi:10.1103/physrevb.79.085203.
35. Itkis ME, Emerling BM, Brill JW. Imaging charge-density-wave strains with electromodulated transmission. Phys Rev B. 1995;52(16):R11545–8. doi:10.1103/physrevb.52.r11545.
36. Roczniak A, Petriu EM, Costache GI. 3-D electromagnetic field modeling based on near field measurements. In: Quality Measurement: The Indispensable Bridge between Theory and Reality: IEEE Instrumentation and Measurement Technology Conference and IMEKO Tec; 1996 Jun 4–6; Brussels, Belgium. p. 1124–7. doi:10.1109/IMTC.1996.507339.
37. Noreika A, Tarvydas P. Electromagnetic field modeling using edge finite elements. In: 11th International Biennial Baltic Electronics Conference; 2008 Oct 6–8; 2008; Tallinn, Estonia. p. 99–102. doi:10.1109/BEC.2008.4657487.
38. Fiodorov NN. Fundamentos de electrodinámica. 2nd ed. Moscow, Russia: Mir Moscow; 1982.
39. Cardenas DE, Ezekoye OA. Thermal characterization of electrical wires and insulation operated in variable frequency mode. Fire Technol. 2015;51(5):1071–92. doi:10.1007/s10694-015-0474-1.
40. Cárdenas D. A "thermal-conductive simplified model" for the actual temperature of overloaded cables. IEEE Lat Am Trans. 2019;17(4):615–24. doi:10.1109/tla.2019.8891886.
41. Cardenas D. Algoritmo de modelo termoconductivo para el cálculo preciso de temperaturas en conductores eléctricos de potencia. Rev Int De Métodos Numéricos Para Cálculo Y Diseño En Ingeniería. 2020;36:1–10. doi:10.23967/j.rimni.2020.01.002.
42. Cardenas Estrada DE. True Calculus of the warming in electrical wires in low voltage: a design correction. IEEE Lat Am Trans. 2015;13(1):172–80. doi:10.1109/tla.2015.7040645.
43. Alberto Gonzalez M, Elam Cardenas D. Analytical expressions for the magnetic field generated by a circular arc filament carrying a direct current. IEEE Access. 2021;9:7483–95. doi:10.1109/access.2020.3044871.
44. Modrić T, Vujević S. Computation of the electric field in the vicinity of overhead power line towers. Electr Power Syst Res. 2016;135(2):68–76. doi:10.1016/j.epsr.2016.03.004.
45. Nicolaou CP, Papadakis AP, Razis PA, Kyriacou GA, Sahalos JN. Measurements and predictions of electric and magnetic fields from power lines. Electr Power Syst Res. 2011;81(5):1107–16. doi:10.1016/j.epsr.2010.12.014.
46. Machado VM, Pedro ME, Brandão Faria JA, Van Dommelen D. Magnetic field analysis of three-conductor bundles in flat and triangular configurations with the inclusion of proximity and skin effects. Electr Power Syst Res. 2011;81(11):2005–14. doi:10.1016/j.epsr.2011.06.010.
47. Karady GG, Nunez CV, Frix W, Maracas KB, Kroese AJ. A novel magnetic field management method for underground power cables. Electr Power Syst Res. 1994;31(2):103–10. doi:10.1016/0378-7796(94)90087-6.
48. Grainger JJ, Stevenson WD. Power system analysis. New York, NY, USA: McGraw Hill; 1994.
49. Kothari DP, Nagrath IJ. Modern power system analysis new. New York, NY, USA: McGraw Hill; 2003.
50. Meeker D. Improvised asymptotic boundary conditions for electrostatic finite elements. IEEE Trans Magn. 2014;50(6):1–9. doi:10.1109/tmag.2014.2300196.
51. Jin JM. The finite element method in electromagnetics. 3rd ed. Hoboken, NJ, USA: John Wiley & Sons, Inc; 2014.
52. Taflove A, Hagness SC, Piket-May M. Computational electromagnetics: the finite-difference time-domain method. In: The electrical engineering handbook. Amsterdam, The Netherlands: Elsevier; 2005. p. 629–70. doi:10.1016/b978-012170960-0/50046-3.
53. Sankaran K. Are you using the right tools in computational electromagnetics? Eng Rep. 2019;1(3):e12041. doi:10.1002/eng2.12041.